**UNIVERSITY OF CALIFORNIA,
IRVINE**

The waterbomb actuator: a new origami-based pneumatic soft muscle.

THESIS

submitted in partial satisfaction of the requirements
for the degree of

MASTER IN INDUSTRIAL ENGINEERING

by

Victor Bogunyà Piferrer

2017

To

my beloved father:

my mentor, my inspiration, my friend.

TABLE OF CONTENTS

LIST OF FIGURES

ACKNOWLEDGMENTS

I would like to express my deepest appreciation to my advisor, Professor David Reinkensmeyer, for his support, enthusiasm and for allowing me to conduct my research with absolute freedom.

I would also like to express my deepest gratitude to the Balsells Fellowship, with an special mention to Pete Balsells and Professor Roger Rangel, for giving me the opportunity to develop my Master's Thesis at the University of California Irvine.

In addition, I want to thank Benjamin Dolan and the RapidThech department for helping me through the 3D printing process.

Finally, I would like to thank my fellows in the Biomechatronics laboratory, my friends, my family and my girlfriend for their constant support and advise.

ABSTRACT OF THE THESIS

This project introduces a new Pneumatic Artificial Muscle (PAM) design based on an origami structure. This artificial muscle is designed to operate at a very low range of pressures while being lightweight and compliant. It is also designed to reduce the pressure threshold and hysteresis problems present on other PAMs like the McKibben actuator. These properties are achieved thanks to a rearranging membrane based on the Waterbomb pattern, which can contract upon inflation while keeping the surface area constant.

This concept has been tested using paper prototypes coated with silicone. We created thee different structures (4x8, 6x12 and 8x16 cells waterbomb actuators) from the same paper sheet (14x28cm^2) and we actuated them under loads of 2, 4 and 7N. The 4x8 was discarded, but the 6x12 and 8x16 actuators contracted a maximum of 12.5% of the original length ($\simeq$10cm) while the operating pressures remained under 5Pa.

We also proposed a novel approach to 3D print these actuators using a Stratasys Objet260 Connex3 3D printer. The main idea consists in creating a flat structure that can self-assemble using a technique known as 4D Printing. The pattern is printed as a flat sheet where the hinges are composites composed of an elastomeric material and shape memory polymer (SMP) fibers. These hinges can be activated through a thermomechanical process inducing a self-folding effect.

Unfortunately, we were not able to verify this fabrication process due to the lack of material availability.

1. INTRODUCTION

1.1. Introduction

Conventional robots and machines are designed to be fast and strong so they can perform repetitive tasks with precision. These features are achieved thanks to the rigid nature of their components, which are usually made with materials like aluminum or steel. Despite being extremely useful, these kinds of robots are usually specialized for a specific task and they don't show the multifunctionality of natural organisms. Furthermore, their rigidity and strength makes them potentially dangerous in case of interaction with humans or other organic elements.

Now, the field of robotics is expanding beyond its classical applications and moving towards fields like cooperative human assistance, healthcare or exploration. This presents new challenges as the classic rigid robot structure is not necessarily safe or compliant enough for these applications.

To fulfill these needs, the Soft Robotics field was born. This field's main goal is to create soft and compliant robots and actuators which are inherently safe and can emulate the properties of natural organisms. It usually relies on soft materials like fluids, gels, soft polymers or easily deformable matter and the designs are highly influenced by nature. These robots must be able to safely interact with natural organisms and adapt to complex and unpredictable environments.

These new soft structures present several challenges. How to power them? Which actuators are suitable for these applications? If they are made with soft materials, are they reliable enough? What is their lifespan? How can they be modelled and controlled when the structure can't be considered a chain of rigid links anymore?

Despite all these new challenges, this field is continuously growing and advancing, producing a variety of new robots for many different applications, like an octopus inspired soft robot arm [1,2], a quadrupedal walking soft robot[3,4], a soft grip for robotic arms[5], an autonomous fish[6] or several hand exoskeletons for rehabilitation purposes[7–10].

1.2. Motivation

This project was born when a simple question was formulated: "Is it possible to 3D print an actuator that can behave as a muscle?".

There are currently many soft actuators which are being studied and whose properties are very promising. Some of them can be easily produced using specific equipment and materials. However, most of these actuators are not commercially available.

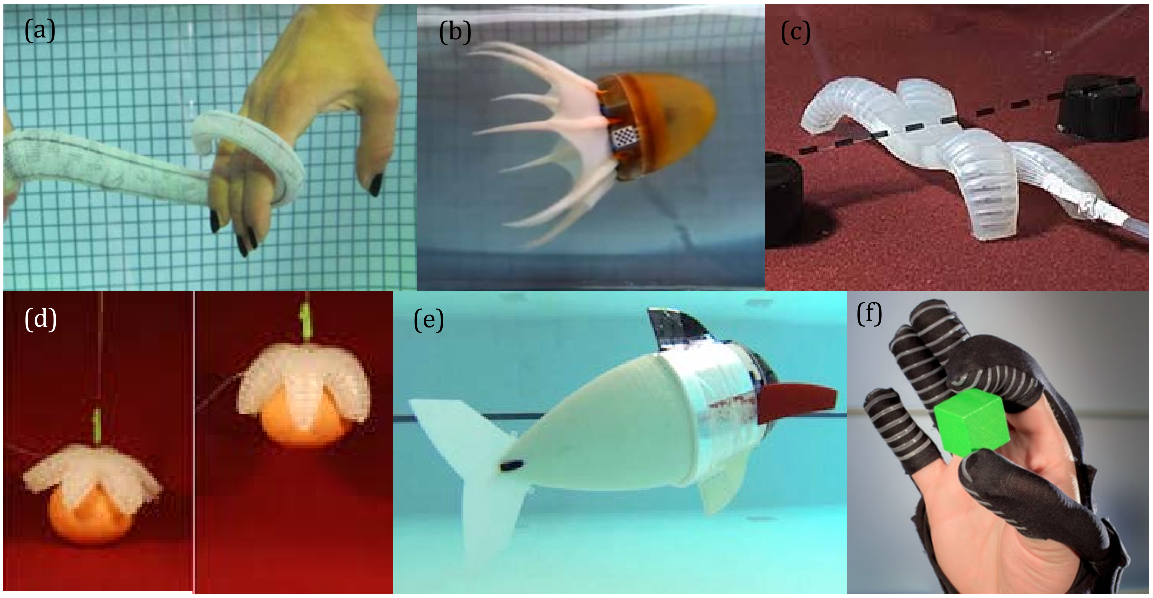

Fig. 1 Examples of soft robots and actuators. (a) Octopus inspired robotic arm. (b) Octopus inspired robot. (c) quadruped soft robot. (d) Soft grip based on PneuNets technology. (e) Autonomous fish robot (f) PneuNets glove for rehabilitation.

Therefore, we hypothesized that a 3D printed contraction device could contribute to the development and spread of soft robotic systems.

Although there are several ways to power a soft actuator, we decided to design a pneumatic actuator. This actuator should be cheap, easy to produce and should contract when actuated. The potential applications for a device with these characteristics could be endless, including exoskeletons, rehabilitation devices or bioinspired robots.

1.3. Objectives

The main goal of this project consists in developing a 3D printable pneumatic soft actuator that resembles the muscular behavior. Having said that, this main goal can be divided in several objectives that will allow us to structure our work and analyze the results.

These objectives are:

1. Collect and review as many pneumatic soft actuator technologies as possible, identifying the materials, principles of operation and characteristics of each actuator.
2. Identify the characteristics we want to endow our actuator with and propose a geometry or design that fulfills these requirements.
3. Verify the contraction properties, the range of pressures and the exerted force of the designed actuator through prototyping and experimentation.
4. Design a CAD model of the actuator that can be 3D printed.
5. Test the final printed actuator to verify its properties.

2. STATE OF THE ART

There are many different technologies that can power a soft actuator. However, in this project we only considered pneumatic devices, as our intention is to produce a pneumatic actuator. In this section, more than 15 different soft actuators will be reviewed. These actuators are classified into two main categories: Pneumatic Artificial Muscles and Soft Pneumatic Actuators.

2.1.Pneumatic Artificial Muscles – PAMs

2.1.1. Introduction and Operation

The Pneumatic Artificial Muscles (PAMs) can be considered the first soft actuators. They became popular in 1950s when the physicist J.L. McKibben used them on an orthotic device designed to help his daughter, who suffered from polio disease[11,12].

At the beginning, this actuator had a limited success due to the challenges of controlling these systems. The non-linear and compliant behavior of the actuator together with the hardware limitations and the pneumatic equipment made those systems hard to control.

However, in the 1980s researchers and manufacturers recovered the interest in this kind of soft actuator because of its compliant properties, simplicity of operation and similarities with biological muscle behavior.

This original actuator, commonly referred as the McKibben actuator, has always been the most popular and widespread PAM. It must be said, though, that other PAMs have been designed, produced and patented through the years.

At present, there are specialized companies like FESTO or SHADOW that commercialize some of these actuators.

Despite the differences and particularities of each actuator, all PAMs rely on the same main principles to operate. The basic design includes two main components: a flexible inner containment layer that exhibits the capacity of large deformation surrounded by a more rigid woven or mesh. When the inner rubber bladder is pressurized, it elastically deforms. Then, the circumferential stress of the inner layer is transformed into axial contraction force by the outer mesh, allowing the actuator to contract upon inflation. Therefore, both the force and motion generated by PAMs are linear and unidirectional.

Darden *et al*[13] explains the operating behavior or any arbitrary PAM through two simple layouts.

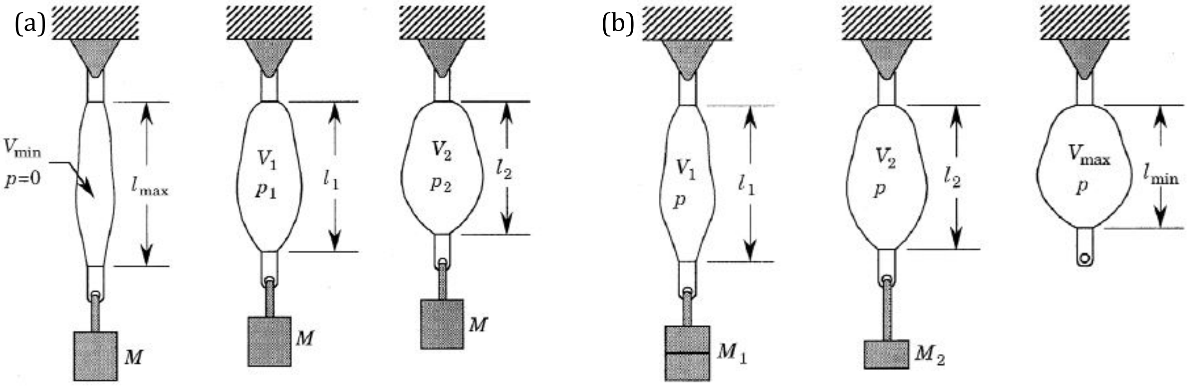

Fig. 2 PAM conceptual experiments: (a) PAM operation at constant load. (b) PAM operation at constant pressure.

The first setup, depicted in Fig. 2 (a), consists in an arbitrary PAM subjected to a constant mass M. At zero-gauge pressure, the volume of the inner bladder is minimal V_0 and it shows the maximal elongation L_{max}. When the actuator is pressurized to a gauge pressure P_1, it will expand and begin to exert a pulling force on the mass. The mass M will be lifted until the generated force is equilibrated with the mass weight, reaching an equilibrium state. This new state will be defined by the membrane's volume V_1, the new length L_1 and the inner pressure P_1.

In the second experiment, Fig. 2 (b), the pressure P remains constant while the mass is reduced. In this scenario, the PAM will inflate while it shortens. If the mass M is completely removed, it will be observed how the inner membrane volume will reach its maximum value V_{max} while the length becomes minimal L_{min}.

This experiments allow us to extrapolate five simple rules that depict any PAM behavior:

1. A PAM shortens by increasing its enclosed volume (it contracts when inflated).
2. A PAM will contract against a constant load if the pneumatic pressure is increased.
3. A PAM will contract at a constant pressure if the load decreases.
4. A PAM will contract until it reaches an upper limit, where the enclosed volume is maximal V_{max} and the developed force is zero.
5. A PAM has an equilibrium length for each pair of pressure and load.

2.1.2. Properties

In the next sections, we will discuss the particularities of the different PAMs. However, there are some general properties and characteristics that are common among all the members of this family of pneumatic actuators:

- Simple Design: as it has been explained before, the main design of a PAM consists in a flexible inner containment layer surrounded by a mesh with the ability to transform the radial forces of the pressurized inner layer into linear force and displacement. This simplicity of design makes them cheaper than other pneumatic actuators like cylinders or bellows.
- Power to weight ratio: these actuators are extremely lightweight as their main component is a rubber or silicone membrane. However, some of them can operate at remarkable high pressures, more than 8 atm.[14] in some cases, allowing them to generate power to weight ratios of several kW/kg. Some of these actuators can lift more than 400 times their own weight (this weight doesn't include all the pneumatic equipment needed to feed the pressurized fluid in the actuator).
- Compliance: the combination of the design together with the compressibility of the air used to power these actuators can guarantee a soft touch and safe interaction. Even when the pressure is maintained at a fixed level, PAMs show a spring-like behavior. This characteristic is what make these actuators so appropriate for applications that require human interaction or fragile objects manipulation.
- Muscle resemblance: experimental results prove that this these actuators usually show force-length properties that are like human muscles. However, it has also been proven that the force-velocity properties don't match muscle well[15]. This partial muscle resemblance makes these actuators suitable for applications like exoskeletons or prosthesis.
- Antagonistic configuration: PAMs generated motion is linear and unidirectional. Therefore, an antagonistic setup is required to generate a bidirectional rage of force and motion, just as many of the skeletal muscles configurations. In this configuration, one actuator moves the load while the other acts like a brake to stop the load at the desired position. The equilibrium positon is defined by the ratio of both muscle pressures[16].
- Connection and replacement: unlike other actuators, PAMs don't require a speed reduction and can be directly connected to the system. It is easy to fit them because they are usually small and they can bend. These properties make them easy to connect and replace.
- Safety: PAMs can be considered safe, not only because of the compliant behavior, but also because they are usually powered with an innocuous gas like air. This means that some hazards like pollution, explosion and electrical shock are totally ruled out. However, some hazard can derivate from the high pressures some actuators can achieve.
- Pneumatic system: PAMs are usually powered by compressed air, although there are some hydraulic designs[17]. This means that the use of these actuators requires pneumatic equipment like valves, pumps and tanks. This is not a problem when the system is meant to remain in laboratory or factory with the proper air source. However, this must be considered when designing mobile or wearable devices.

- Service life: There is not an extensive study about the durability of PAMs even though the durability of the rubbery membrane is one of the main concerns when using them. It has been reported that some PAMs break where the flexible membrane is connected to the rigid end fittings due to stress concentrations. It has also been reported how the friction between the soft and the rigid layers has created significant deterioration. Shadow Robot Company suggest that their S30AM-S-1 muscle should be kept in the 0-20% of the contraction range as "The less they bulge, the longer they last"[18]. (Its maximum contraction is 37% of the original length)
- Control: Despite the attractive advantages, PMAs usually have high nonlinear properties and hysteretic characteristics which are produced by air complexity and nonlinearity of its own geometric construction, as well as friction in the mesh[19]. This creates an important challenge when trying to control the system properly. This control problem has been approached using a variety of different solutions, as classic PID control, including several variations[20], Adaptive Neural Network control [19,21] and non-linear control approaches, like sliding-mode[22], among others.

2.1.3. Classification and Description

Since the McKibben actuator was popularized, several new PAMs have been designed and produced. There are different criteria that can be used to classify these actuators, like the operational fluid (pneumatic or hydraulic), the range of pressures (overpressure or underpressure), the nature of the rigid layer (braided, netted or embedded membrane) and the elastic abilities of the membrane (stretching membrane or rearranging membrane).

Daerden *et al*.[13] proposed a four-group classification:

Braided Muscles:

The basic structure of a Braided muscles consists in an inner air-tight elastic tube or bladder surrounded by a braided sleeve which fibers run helically around the muscle axis with a +θ and – θ pitch or angle. When the tube is pressurized, it expands and presses against the braided sleeve. Then the fiber tension is balanced with the external load, allowing the muscle to contract in the axial direction while expanding in the radial direction, always keeping a cylindrical shape.

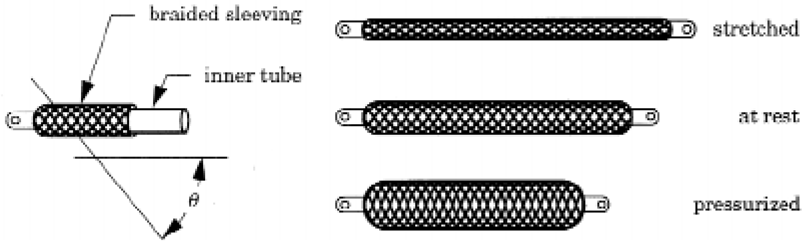

Fig. 3 Braided muscles structure and operation

There are two main braided muscles, which are distinguished by the way the rubber bladder is attached to the sleeve.

- **McKibben Muscle:** this type is the most common PAM since it was used in the 1950s by J.L. McKibben. It should be said, though, that he is not considered the inventor of this actuator[12]. It consists in a bladder and a sleeve which are both connected at both ends to fittings that serve both as an airproof enclosure for the bladder as well as a stress transmitter between the sleeve and the external load.
  The bladder is usually made of rubber or latex while the sleeve is made with Nylon or other fabrics. The final properties of the actuator, like the range of contraction-extension, are very related with the chosen materials and the sleeve's fiber angle.
  The maximum contraction of a McKibben is around 25-30% of its maximum length, while the power to weight ratio can range between 1.5kW/kg and 10kW/kg[13].
  The regular weight of this actuator can range between 10 and 150g[18].
  For instance, the Shadow S30AM-S-1 is a 30mm actuator that weights 80g and can contract by up to 37%, although the manufacturer suggests keeping the contraction ratio under 20% to prolongate the lifespan. This specific actuator can produce forces of 700N at 3.5bar.
  Furthermore, this actuator has been studied along the years and there are plenty of models that describe its behavior[11,12,23,24]. Most models take into consideration two main facts that happen while operating this actuator. The first one is known as threshold pressure and it refers to the minimum pressure required to start the radial deformation of the bladder. It is mainly caused because of the initial resistance of the bladder to inflate. The second is known as hysteresis and it refers to the difference in the contraction ratio for the same pressure and load that can be observed in the contraction and elongation processes. It is mainly caused by the friction between the bladder and the sleeve.
  As it has been already said, this actuator is the most common among PAMs. This is mainly because its simple design, easy assembly and low cost. However, the service life of this actuator seems not very high, for the reasons already explained in the previous section.

Fig. 4 McKibben actuator at rest and pressurized

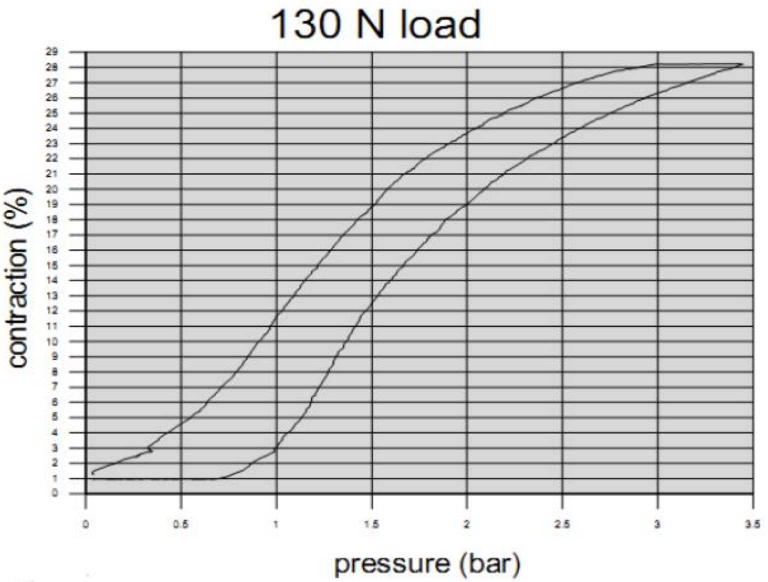

Fig. 5 Pressure-Contraction graph for a Shadow S30AM-S-1 under a 130N load. Both the pressure threshold and hysteresis phenomena can be observed.

- **Sleeved Bladder Muscle:** this actuator is very similar in construction to the McKibben actuator and it uses the same materials for the bladder and the sleeve. The main difference is that the inner bladder is not connected to the sleeve in both endings. That means that the fittings located at both ends of the actuator only serve as a stress transmitter between the fibers and the load. This design allows the elimination of the passive spring force present in the McKibben design due to the rubbery bladder being connected to both extremes.

Netted Muscles:

The main difference between netted and braided muscles is the significant difference in the densities of the network that surrounds the bladder. While braided muscle sleeves are tightly woven, netted muscles have a net with relatively large holes. This allows them to reduce the friction between the bladder and the net, and thus, the hysteresis. Furthermore, the actuators related to this group are usually the rearranging kind, which means that the bladder is meant to rearrange but not stretch and thus, reduces the threshold pressure. These characteristics makes them easier to control as well as optimize the pressure required to operate them.

There are three main designs.

- **Yarlott Muscle:** this PAM patented by J.M. Yarlott[25] consist in a bladder with an elongated spherical shape (shaped like a football ball) which is covered by several cords that are placed over the bladder's surface axially, from end to end. The main purpose of this axial cords is to transform the radial pressure exert by the bladder into axial force and motion. A second set of cords runs the actuator's surface perpendicularly to the axis direction, connecting the longitudinal strands. The main purpose of this strands in to reinforce the bladder to resist elastic expansion. When the actuator is fully extended, the longitudinal cords are completely straightened creating a star-like folded pattern in the surface. When compressed, the actuator takes a prolate spheroidal shape. This actuator was designed to operate at a low range of pressures (up to 1.7kPa).

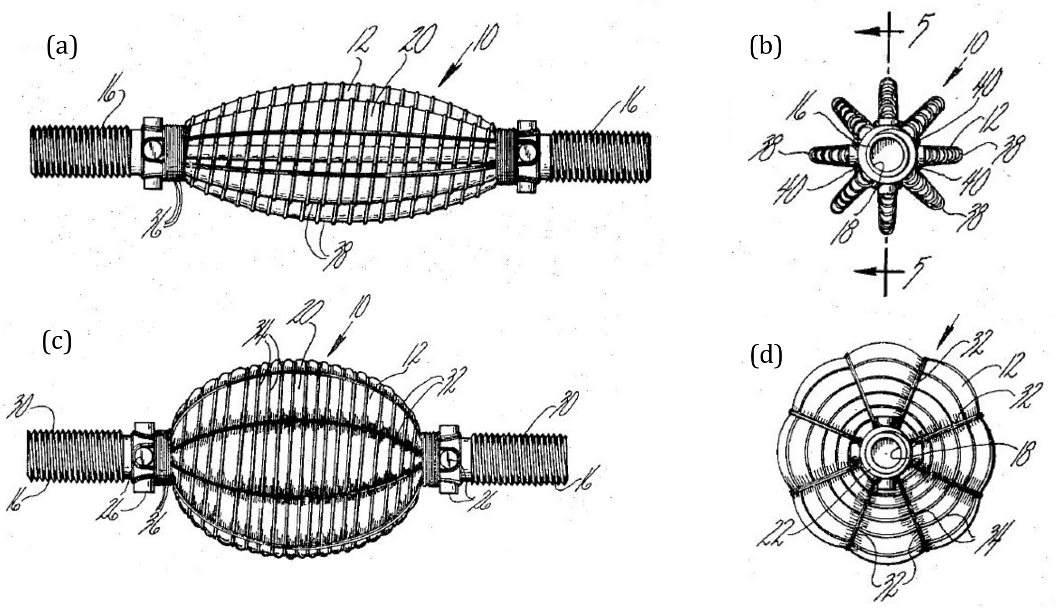

Fig. 6 Details of the Yarlott muscle geometry showed in the US Patent No. 3645173. Figures (a) and (b) show the actuator in the resting position while (c) and (d) show the contracted actuator.

- **ROMAC:** The RObotic Muscle ACtuator (ROMAC) was patented by Immega and Kukolj in 1990[26]. It consists in a harness composed of rigid straight wires interconnected by nodes creating a very specific geometry which can expand in the radial direction while contracting in the axial one. The harness covers an airtight bladder which is flexible but doesn't stretch too much. This design allows the actuator to change the volume keeping the total surface almost constant, due to the membrane's tensile stiffness. The absence of friction and membrane stretching is translated into a lower hysteresis and higher exerted force than braided muscles.
  The length of this actuator ranges between 6cm and 30cm, although there is a miniature version of 1-6cm. For a regular size, a 50% of contraction has been reported under pressures up to 700kPa while exerting forces between 4500N and 13600N.

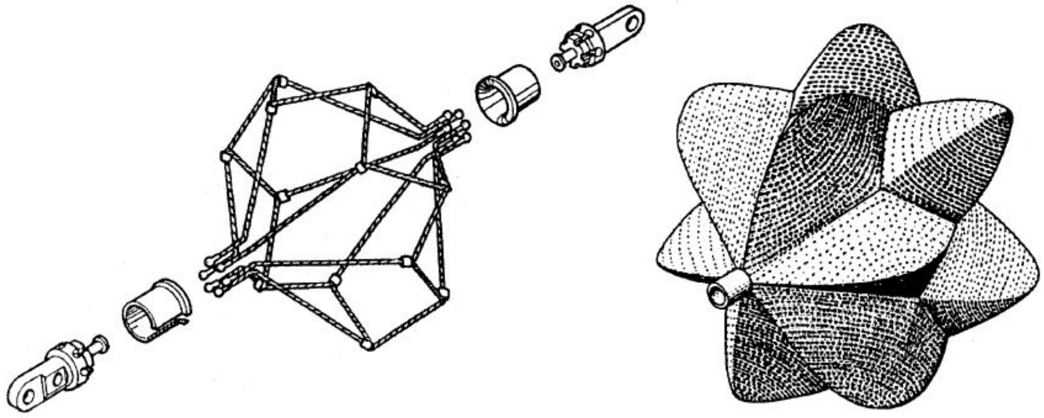

Fig. 7 The ROMAC (RObotic Muscle ACtuator). The wire rigid structure is showed in (a) while (b) depicts the final shape once it is covered with the bladder

- **Kukolj Muscle:** this PAM, patented in 1988by M. Kukolj[27], consist of a tubular bladder which is similar to the McKibben muscle one. This bladder is surrounded by a helicoidal open-meshed net that runs axially without being in contact with the bladder except in the ends. This creates a significant gap between the net and the bladder which is meant to eliminate the buckling effect due to the tendency of the network to contract faster than the membrane.

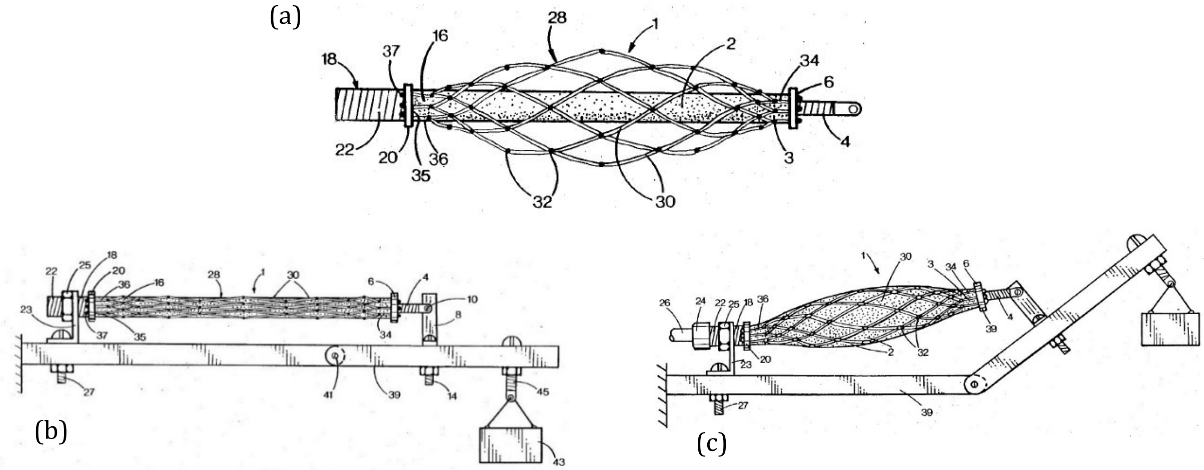

Fig. 8 Details of the Kukolj muscle geometry and operation showed in the US Patent No. 4733603. (a) shows the actuator in the resting position, (b) shows the actuator at its maximum length under a certain load and (c) depicts the pressurized actuator lifting a load.

Pleated Pneumatic Artificial Muscles (PPAM):

This design was introduced by Daerden at the early 2000s[13,28]. The main characteristic of this design is that the membrane is not meant to stretch under pressurization, but only to rearrange. This is achieved by sealing a Kevlar 49 fabric with a polypropylene lining, obtaining an airtight rigid membrane. This membrane is folded in several pleats in the actuator's axial direction. When the PAM is pressurized, the membrane unfolds without stretching, obtaining a final spherical shape that resembles a pumpkin. Therefore, this actuator can be classified as a rearranging membrane actuator as well as an embedded membrane actuator. However, the shortening effect is not a direct consequence of the interaction between layers but because of the folding pattern.

The fact that this actuator can inflate without stretching the bladder material grants him with very interesting properties. First, as no material is stretched, there is almost no threshold pressure. Furthermore, as the expansion process involves almost no friction between the two layers, there is almost no hysteresis. These facts make this design more reliable and easy to control. However, its main problem is related with the shape. Instead of keeping a cylindrical shape like the McKibben, it turns spherical when inflated, which makes it harder to place in certain designs.

Experimental results show contractions up to 41.5% of the maximum length for a 10cm actuator that weights 60g. The pressure was limited to 300kPa and the load was 3500N.

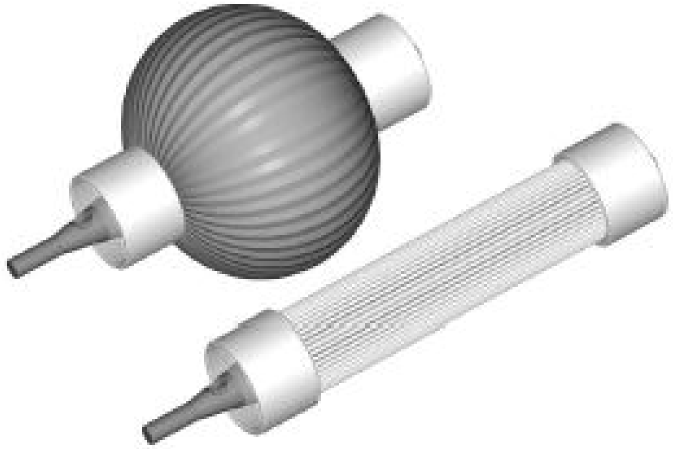

Fig. 9 Daerden Pleated Pneumatic Artificial Muscle

Embedded Muscles:

The main characteristic that defines these actuators is that, unlike braided and netted muscles, the rigid layer is embedded inside the bladder. This allows them to reduce the friction, making them more reliable and easy to control. There are a lot of known actuators in this category but we only will mention a few.

- **Baldwin muscle:** this actuator is based on the design of another actuator, the Morin actuator, which can't be considered a pneumatic muscle. It consists in a very thin rubber membrane with elastomeric properties which has embedded glass filaments in the axial direction. This configuration makes it have a higher elastic modulus on the axial direction that the radial one.
  The thin membrane together with the absence of friction provide this actuator with very low hysteresis and threshold pressures. However, because of the thin membrane, the gauge pressures must be kept at low values, no more than 100kPa. Some test indicates an operating life between 10.000 and 30.000 cycles working at 100kPa and a load of 45kg[29].

- **UPAM:** the UPAM, or Underpressure Pneumatic Artificial Muscle, is one of the few artificial muscles that are actuated by removing the air inside the bladder, creating a negative pressure respect the environment. When actuated, this muscle squeezes in a non-symmetrical way, becoming flat in the middle area.
  The maximum underpressure is around 100kPa and the maximum contraction is around 20% for 100mm length and 50mm diameter actuators[13].

- **Paynter Knitted Muscle:** this actuator consists in a knitted net of strong and flexible fibers embedded in a spherical elastomeric bladder. When the actuator is set under a load, it elongates and when it is pressurized it recovers the original spherical shape.
  It is designed to work at high pressures, up to 8.3 atm.[14]

- **Paynter Hyperboloid Muscle:** This actuator is characterized by the shape it takes when is fully elongated: a hyperboloid of revolution[30]. This shape is achieved because of its construction. A set of flexible but inextensible threads are secured in the end fitting with a specific distribution. This threats are then embedded in an elastomeric bladder. When this actuator is pressurized it takes a spherical shape.

2.2. Soft Pneumatic Actuators – SPAs

2.2.1. Introduction and Operation

In recent years, a new family of highly compliant pneumatic actuators have been developed. This new family of actuators is commonly known as Soft Pneumatic Actuators (SPAs). Their main characteristic, which differentiates them from other pneumatic actuators like PMAs, is that they are almost entirely made from soft materials such as silicones or rubbers. This makes them lightweight, inexpensive and easy to produce.

The basic SPA design consists in a main silicone body which contains one or more air chambers connected by an air feeding channel. The chambers are designed to have two opposing walls, one of them being more rigid than the other.

When pressurized, the chambers expand by stretching the regions that are more compliant or have less stiffness. In order to accommodate the asymmetric elongation caused by the difference of stiffness of opposing walls, the structure bends around the inextensible layer. Therefore, the main movement these actuators produce consist in a “gripping” motion or bending torque, so the distance between the two ends of the actuator decreases as the curvature increases.

In homogenous designs (actuators made entirely of rubber or silicone), the difference of stiffness is achieved by creating walls with different thicknesses. The thinnest layers of rubber tend to stretch more that the thicker ones. In the case of heterogeneous designs, a layer of a more rigid material like paper or fabric is embedded in the silicone walls. The resulting composite wall has very little planar strain while keeping the touch and airtight properties of the silicone or rubber.

The designs that contains more than one chamber embedded in the silicone are commonly known as PneuNets (Pneumatic Networks).

2.2.2. Properties

Every SPA has its own characteristics, and they will be explained in detail in the following section. However, some of these properties are common among all this family members:

- Soft materials: as it has been explained before, the main and foremost characteristic that defines these actuators is that they are almost entirely build of soft materials like silicone. Some commercial silicones have been used for this purpose, such as Smooth-on Ecoflex 00-30[5,31–33], Elastosil M460[33] and Dow Corning Sylgard 184 Silicone[5]. These silicones are usually cheap and easy to manipulate.
  Is some cases, some rigid material can be embedded in the silicone to endow a wall with rigidity or reinforce certain areas. This material is usually paper, although some fabrics and other materials can be used too.

- Simple Design and production: the intrinsic simplicity of the design and the materials used, make the production process quite simple. The SPA is commonly designed using a CAD software, which allows to specify the geometric dimensions of the inner chambers and air channels. Then a negative mold of the design is produced, usually with a 3D printer. Finally, the silicone is poured into the mold and the reinforcements are embedded while the silicone is in a liquid state.

  In the case of SPAs with only one chamber, only one mold is required. The final shape is accomplished by pouring the silicone in a mold with the external SPA shape while a rigid piece with the inner chamber shape is introduced in the mold in order to create the inner walls[34]. In the case of PneuNets (multiple chambers), two molds are usually required: one mold is used to cast the soft part of the actuator (the one that contains the chambers and channels while the other is used to cast the layer embedded with the rigid material. Then, the two parts are glued together with the same silicone used to cast them[31,33].
- Pressure range and Pneumatic hardware: these actuators rely on the hyperelastic behavior of the silicone to operate. This limits the range of pressures which these actuators can operate. The maximum pressure associated with SPAs is usually around 50kPa, but often lower. If higher pressures are desired, the walls have to be designed thicker, which hinders the bending process.

  On the other hand, the fact that the required operating pressure is low, makes easier to create small, light, portable pneumatic sources to feed them[32].

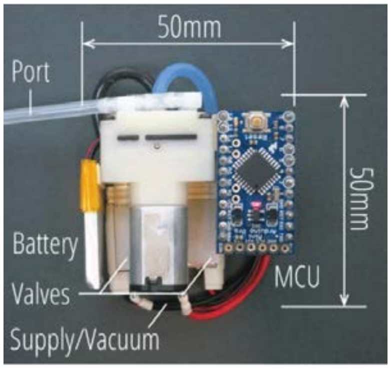

Fig. 10 Miniature pneumatic control system composed by two solenoid valves (SMC, Series S070), a Koge Electronics pump (Series KVP), a lithium battery (3.4V, 110mAh) and an Arduino Nano board.

- Safety: SPMs can be considered very safe for several reasons: their soft touch and compliant behavior makes them ideal for applications that require human interaction, the range of operation pressures and exerted forces is so low so they don’t represent a risk and, finally, they are powered with an innocuous gas. This means that some hazards like pollution, explosion and electrical shock are discarded.

- Compliance, modeling and Control: As these actuators are mainly made with silicone and powered with compressed air, they are extremely compliant. In part, this makes them hard to control with precision. However, these actuators are used in applications that don't require a precise position control but a compliant behavior, like grasping irregular objects. Furthermore, it is hard to model these actuators due to the compliant materials which they are made of. This is why a Finite Element Software like ABAQUS or ANSYS can be used during the actuator's design stage so the final deformed shape for a specific pressure is the required.
- Finger resemblance: the bending motion associated with these actuator makes them appropriate for applications that require a finger-like actuator. That is the reason why it has been used is several hand exoskeletons[7–10] and robotic hands[35,36].
- Service life: these actuators rely on the high deformation of silicone to operate. However, stretching the silicone repeatedly shortens significantly its lifespan, making the actuator susceptible to fail after a low number of cycles. Furthermore, some air bubbles can be introduced into the rubber during the casting process, which can create concentrated stresses that weaken the wall and lead to premature rupture. This can be mitigated by degassing the liquid silicon before curing it.
- Embedded sensing: another interesting property of SPAs is that some sensors can be embedded in the silicone during the fabrication process in order to detect deformation or pressure. One of the most known techniques consist in injecting a conductive liquid metal (eGaIn) into microchannels embedded in the elastomer. When the SPA is actuated, the geometry of the microchannels is modified and the liquid metal responds by changing its resistance[37].

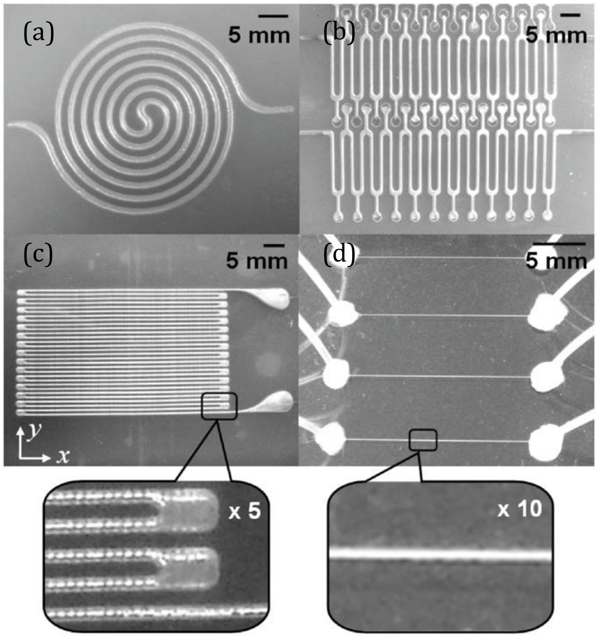

Fig. 11 Embedded eGaIn sensors. (a) (b) Pressure sensors, (c) (d) strain sensors.

2.2.3. Classification and Description

In this section, we will present the most common SPAs and some of their variations. In order to maintain coherence and order, we have classified all these actuators in three main groups: PneuNets, Fiber reinforced and Elastic Airbags.

Pneumatic Networks

As it has been already explained, a PneuNet actuator is an SPA almost entirely made with silicone which design consist in multiple chambers connected by an air feeding channel. Each single chamber has the ability to bend when pressurized due to the asymmetry of elongations in opposing walls. The final bending motion is the result of the additive deformation of all chambers.

- **Bending SPA:** this is the most common Soft Pneumatic Actuator and it has been used for multiple applications such as gripper with a starfish-like structure[5,38] or a walking soft robot[3].
  In this design, all chambers are embedded in a solid piece of silicone, which have its base reinforced which a continuous piece of paper or fabric. All contiguous chambers are separated by a solid wall of silicone. When the actuator is pressurized, the upper wall (the wall that opposing the reinforced one) stretches considerably more than the other walls, creating the curling motion.
  According to Mosadegh *et al.*[33] , the performance of a PneuNet can be classified into 5 parameters: i) bending speed ii) exerted force at a given pressure, iii) change of volume required to achieve certain bending, iv) actuation cycles without failing and v) correlation between the pressure and the degree of bending without load.
  It must be said that these parameters can vary significantly due to differences in materials, wall thickness or design.
  Mosadegh *et al.*[33] tested a 15 chamber SPA with 1mm wall thickness and 10.5mm chamber height. They reported that this actuator can bend 41º at 72kPa, applying a force of 1N at this pressure. The time required for full deformation is 3.3s while being actuated by a BTC-IIS miniature compressor. This actuator failed, on average, after 126 cycles actuated at 0.33Hz.
  Sun *et al.*[31] tested a 10 chamber SPA, each chamber being 2mm width, 4mm height and 8mm length. They tested several wall thicknesses: 2,3 and 4mm, achieving a maximum force of 4.2N for the 4mm thick wall working at 50kPa. It must be said that their results show that actuators output force decreases when the deformation increases. This have a huge resemblance with the muscular-alike properties of PMAs.
  The 3 and 4mm wall thickness actuators fully bend in 5 and 7 seconds under a 40kPA increment of pressure. When the actuators are depressurized, they take approximately 3 seconds to return to the original shape.

Although these actuators are airtight, there are leaks that will make the actuator deflate passed a certain amount of time. Ilievski *et al.*[5] reported that their starfish-like gripper could maintain the shape for 10 minutes, although it required 60 minutes for full deflation.

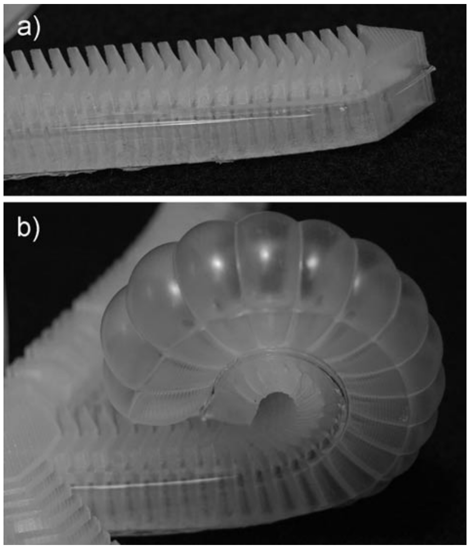

Fig. 12 Example of bending SPA. In this case, the base of the SPA has an improved pattern to favor the gripping function

- **Fast Bending SPA:** One of the main problems when using the previous actuator is the slow actuation speed, the short lifespan and the large change of volume required for full actuation. That is the reason why, in 2014, Mosadegh *et al.*[33] suggested an improved version of this design that allows to overcome all these defects.
  They named this actuator Fast PneuNet (fPN) but we will refer to it as Fast Bending SPA to avoid confusion.
  The design is similar to the conventional bending SPA with two main differences. The first improvement is the walls that separate chambers are no longer a solid silicone walls. In this case, each chamber has its own walls which are separated from the contiguous chamber ones, leaving a gap between chambers. The second improvement is that the upper wall (the one which opposes the reinforced wall) is considerably thicker than the original design.
  The main idea behind this design is that the same bending movement can be achieved with less stretch and stress in the silicone. When the actuator is pressurized, the upper walls remain almost unstretched because of their thickness, while the side walls deform filling the gaps between them and exerting pressure on each other. This pressure between colliding walls, together with the rigidity of the reinforced base, is what creates the bending motion.

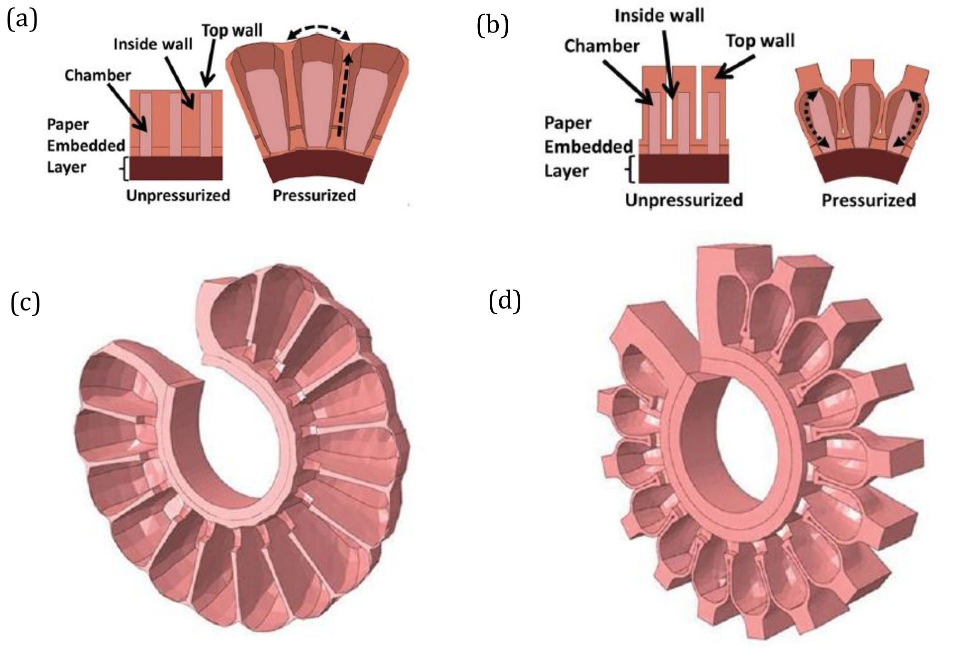

Fig. 13 Comparison between a regular bending SPA and a fast bending SPA. Wile the regular bending spa (a)(c) stretches its upper walls, the fast bending SPA (b)(d) bends by exerting pressure between the coliding walls.

This design allows to apply less strain and stress to the silicone, allowing a considerably longer lifespan, a fastest actuation speed and less volume deformation.
Mosadegh *et al.*[33] tested some 15 chamber fast bending SPA and regular bending SPA with 1mm wall thickness and 10.5mm chamber height. The fPN fully bends in 130ms, more than 25 times faster than the standard homologous. At 72kPa, the fPN reached its full range of motion (360º bending) and the applied force at this pressure was 1.4N, 40% more than the standard design. The increase of the chambers volume is 8 times smaller, making this actuator more efficient as it requires less air volume to operate.
Furthermore, this actuator didn't fail after 10^6 cycles of actuation at 2Hz.

- **Nematode Actuator:** this actuator is a miniaturized version of the standard bending SPA[39,40]. It was developed as a solution for medical and biotechnology fields, being though as an effective way to help in minimally invasive surgery or handling delicate biological samples.
  This specific design has 12 chambers, the length is 15mm and the diameter 2mm.
  It is produced the same way that the standard version, although they don't use paper or fabric to reinforce the non-stretchable wall of the design. This actuator reaches the maximum deformation at 40kPa.

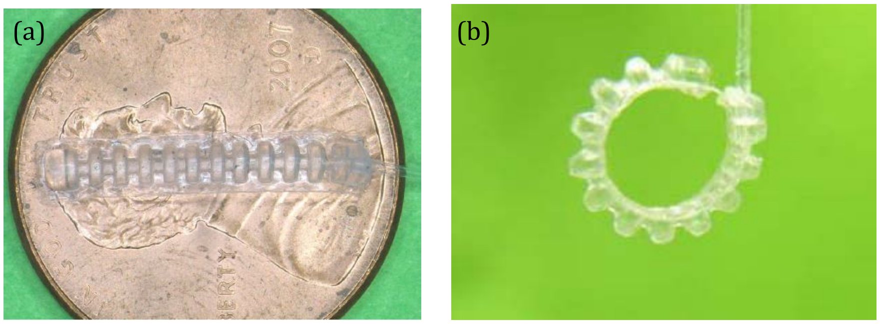

Fig. 14 Nematode actuator. (a) Comparasion between the nematode actuator and a coin. (b) Nematode actuator pressurized at 35kPa.

- **Rotary SPA:** this actuator was introduced by Sun *et al.*[31] and it is presented as an actuator that can be useful for applications requiring an angular displacement of 0-90º. Its design consists in a series of pie-shaped rubber bodies (10º internal angle) containing a chamber. Each body part is connected to the next trough a layer of silicone reinforced with fabric. When the actuator is pressurized, the larger face of the pie-shaped body deforms while the connected reinforced walls remain unstretched. This creates a rotary motion.
  In this paper[31], several 3 chamber actuators with different wall thicknesses (2,3 and 4mm) have been tested.
  The maximum angular displacement at 30kPa is 91º, 82º and 69º for the 2mm, 3mm and 4mm wall thickness samples, respectively.
  Both the 3 and 4mm wall designs can bear pressures up to 40kPa with a maximum torque of 1538.1Nmm for the 3mm case.

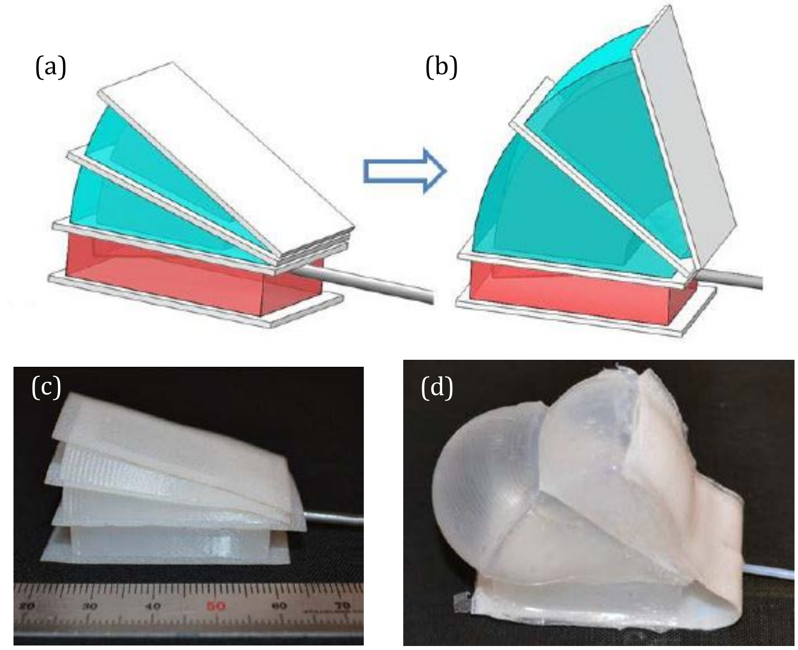

Fig. 15 Rotary SPA. (a) and (b) show a schematic of this actuator's operation. (c) and (d) show the same operation process with a real actuator being pressurized at 25kPa

Fiber reinforced SPA

The Fiber Reinforced SPA is a family of soft bending actuators which main characteristic is that their bending radius and axis can be easily programmed by modifying their structure.

As any SPA, it is mainly made of silicone. However, it differs from other actuator designs in the fact that instead of using only one reinforcement in the base to produce the bending motion, it uses up to three different reinforcements.

The main design consists in silicon body with a semi-cylindrical shape which contains one continuous air chamber. This basic body is reinforced in the base (the flat part of the semi-cylinder) with a continuous fabric to prevent stretching, and thus creating a bending motion. A second fiber, usually in the shape of a thread, is wound around the length of the actuator to constrain radial swelling during pressurization. Finally, a third reinforcement is applied is the form of a sleeve covering the actuator. This sleeve acts as strain limiting layer in all directions, and significantly reduces the covered parts ability to bend. The bending axis can be programed by cutting the sleeve where the bending is wanted to happen. The bending radius can be programmed by the non-covered space between sleeves.

The fabrication process is explained in different publications[34,41]. A mold is used to cast the main silicone body. Then they use woven fiberglass to reinforce the base and a single Kevlar thread is wound around the main body with a 3mm pitch. It must be mentioned that the casted silicone body already had the thread path defined on the surface (it is defined in the mold). Then, another mold is used to encapsulate these reinforcements in a layer of silicone. Finally, a polyolefin/polyester woven fabric that shrinks when heated is used as a sleeve. The sleeve is heated so it accommodates to the actuator's irregular surface.

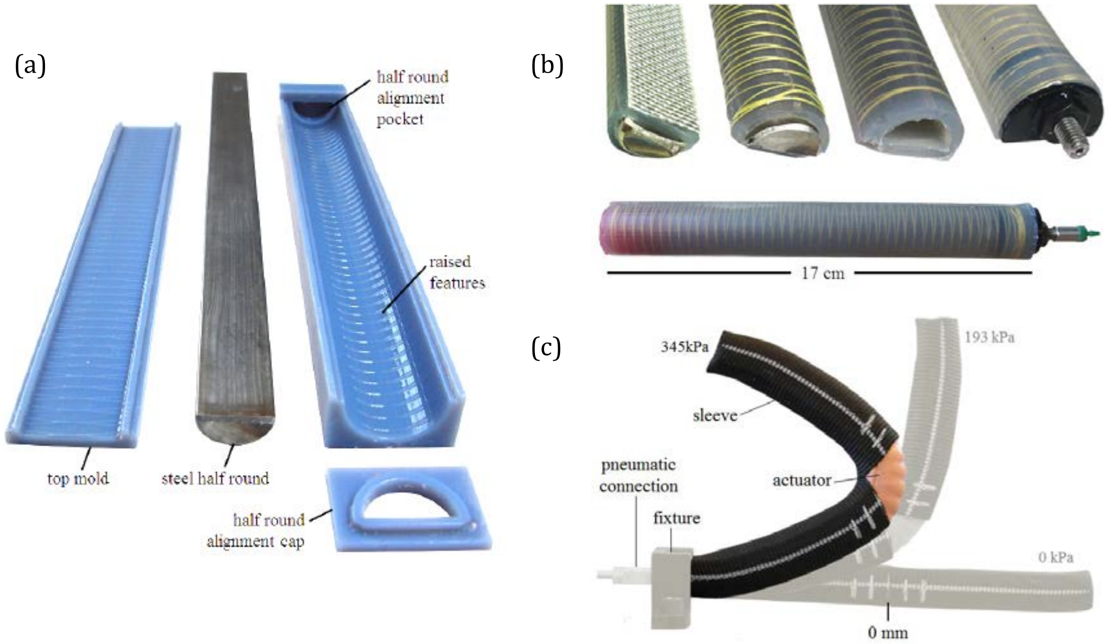

Fig. 16 Fabrication process for a fiber-reinforced actuator. (a) Mold used to cast the silicone main body. (b) This picture shows both the fiberglass reinforced base and the Kevlar thread reinforcement. It also shows how both these reinforcements are embedded in a layer of silicone to protect them. (c) fiber-reinforced actuator covered with the sleeve. Both the bending ratio and axis are programmed by the cut on the sleeve.

In one publication[41], they produced two 16cm actuators, one with a 10A hardness silicone and another one with a 28A hardness silicone. Both actuators weighted less than 45g. The first one was able to operate up to 207kPa while the second reached 414kPa.

They were able to mechanically program the actuator so it remains straight in the sleeved section while achieving precise angles (90º) in some specific non-sleeved areas.

Pneumatic Balloon Actuators (PBA)

This family of soft actuators is also known as Elastic Airbags or Pouch Motors and it differs considerably from the previous ones both in construction and the actuation.

The basic structure of this actuator consists in two thin flexible films bonded together along their surrounding edges, forming a cavity between them. By combining different materials, two different modes of actuation can be achieved.

Konishi *et al.*[42] describes an actuator consisting in a polyamide layer covered with a silicone rubber film bonded together with silicone rubber glue. When the cavity between layers is pressurized, the silicone layer membrane stretches while the polyamide substrate only bends, obtaining thus a bending motion. Yao *et al.*[32] presents a similar structure made with silicone and paper.

Apart from the bending actuator, a linear contraction actuator can also be created[43]. In this case, two flat layers with the same elastic properties are bonded together. When the cavity is pressurized both layers bend without stretching. Therefore, the actuator contracts.

These actuators, specially the bending one, are appropriate for applications that require a bending motion between two flat surfaces. It must be said, though, that the maximum angle between surfaces will be around 90º. Niiyama *et al.*[43] reported maximum angles around 1.8 rad (100º) working at 10kPa. They also reported forced of almost 50N at 20kPa. As the majority of soft actuators, the force these actuators exert is maximum at the beginning of the movement at it is reduced considerably wile it bends.

Niiyama *et al.*[43] used these actuators to power three basic paper robots: a gripper, a robot arm and a legged robot.

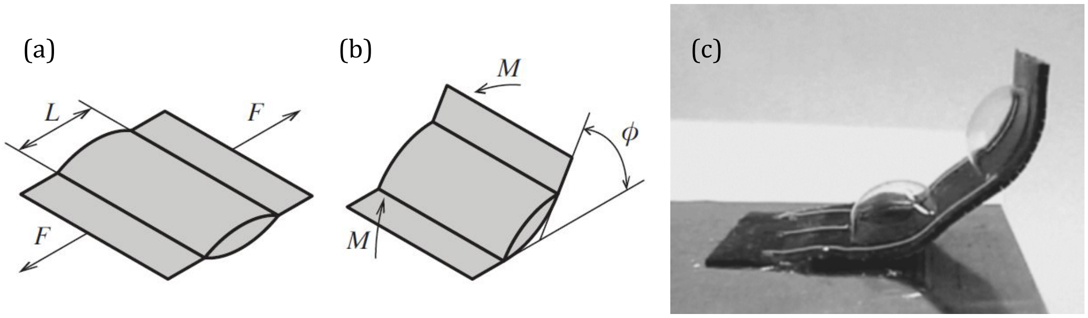

Fig. 17 Pneumatic Balloon Actuators. (a) Linear contraction PBA representation. (b) Bending PBA representation. (c) Pressurized bending PBA

3. CONCEPTIALIZATION

In the introduction, we defined that the main goal of this project is to design a pneumatic soft actuator that can contract upon inflation. However, before proceeding to design any actuator, we need to define the properties and characteristics we want to endow it with.

The first consideration that must be done is the properties of the 3D printer that will be used: the Stratasys Objet260 Connex3. This 3D printer is one of the few 3D printers that can print both rigid materials and rubbery materials. This is a basic required feature as almost all the reviewed soft pneumatic actuators rely on a combination of rigid and rubbery materials to operate. It must be mentioned, though, that the mechanical properties of the 3D printed rubbery materials are considerably worse than other rubbers or silicones. The printed rubbery material presents anisotropic properties as it only prints in one direction, it can’t be subjected to large deformations, no more than 220% of the original length, and it tends to tear apart easier than casted silicones or other rubbers. This 3D printer and its properties and its materials will be fully reviewed in further sections.

Considering the limitations of the 3D printed rubbery material, any design that relies on large deformations should be discarded. Furthermore, designs like the McKibben actuator that present lots of friction between layers should be also ruled out, as the printed materials tend to degrade faster.

Considering this, we believe that the best option would be a rearranging membrane actuator, like the Dearden PPAM or the ROMAC. This 3D printed actuator should be able to contract upon inflation by rearranging its membrane, always keeping its surface area constant.

Although we could have tried to reproduce these mentioned actuators using a 3D printer, we came up with a novel design which is inspired on the ancient art of Origami.

Origami is an art form which was originated in Asian countries like Japan and China. It consists on creating shapes and sculptures with a single sheet of paper folded and sculpted several times. Although it was originally conceived as an art form, nowadays it has become a major inspiration for new ideas and designs in a variety of fields[44] like architecture[45], biomedicine[46], electronics[47] and robotics[48,49].

Our design is based on the well know waterbomb pattern. This pattern consists in folding a single sheet of paper into an array of hourglass-like cells which presents a very interesting property: it is an auxetic surface. An auxetic surface is a structure which presents a negative Poisson ratio so, when it is stretched in one direction, it expands in the perpendicular direction instead of contracting.

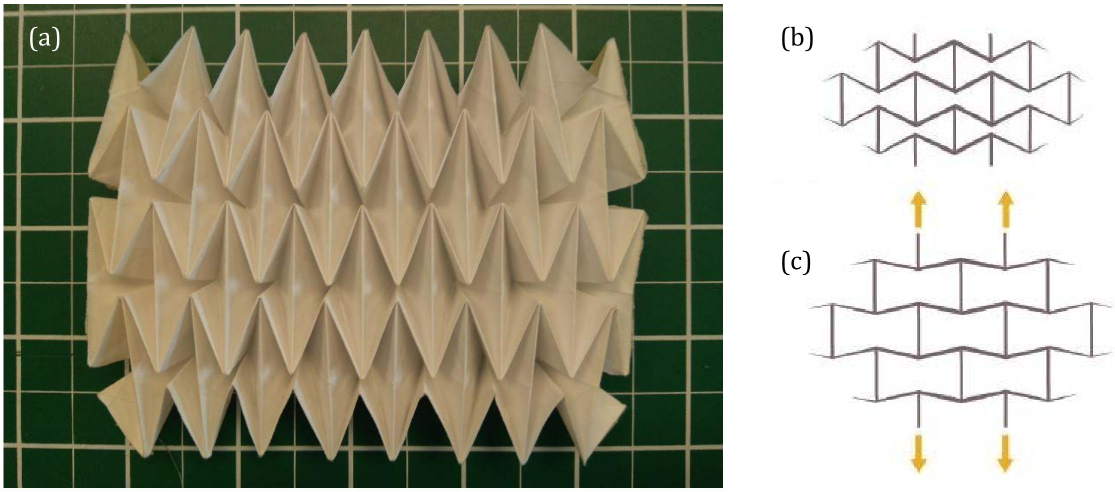

Fig. 18 The Waterbomb pattern. (a) 4x8 waterbomb pattern folded from a 12cm x 24cm piece of paper. (b)(c) characterization of the water bomb pattern's auxetic properties. When this surface is stretched in the direction parallel to the largest hinges of the hourglass pattern, each cell transition from the hourglass shape to a square shape, increasing the covered area in both stretching the direction and its perpendicular.

This surface can be folded upon itself and its short margins can be glued together creating a structure commonly known as the "Magic Ball". This new structure can change its shape from tubular configuration to a wheel shape without changing its surface area. This "Magic Ball" configuration can act as rearranging membrane PMA, which not only should contract but also should have less hysteresis and pressure threshold than other actuators like the McKibben.

Both the waterbomb pattern and the "Magic Ball" configuration have been widely studied and modelled[50–52]. This specific pattern has inspired many applications like a Stent for minimal invasive surgery[46], a battery design[47], a soft worm-like robot[48] or a deformable wheel for soft robots[49]. It has also been actuated using a magneto-active elastomer[53].

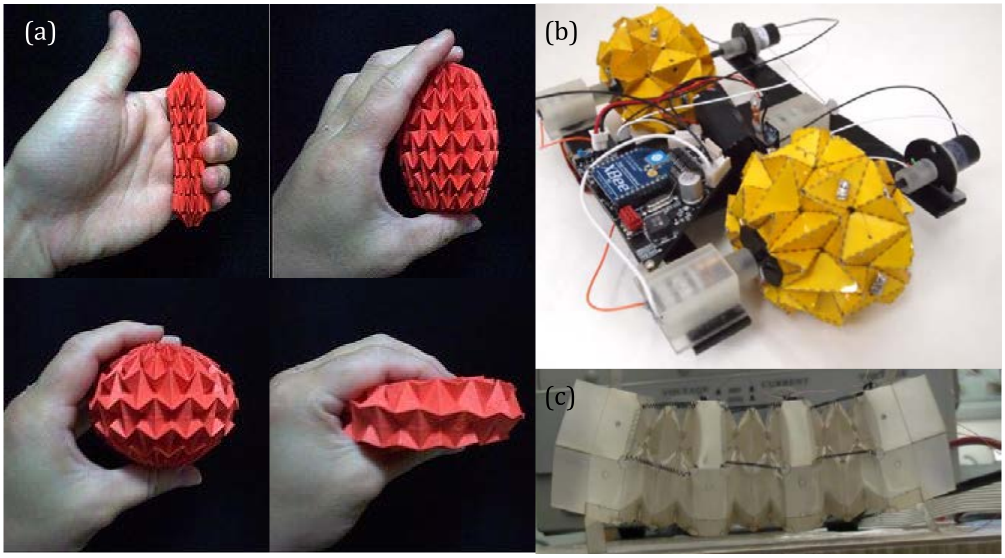

Fig. 19 The waterbomb pattern in the "Magic Ball" configuration (a). (b)Deformable wheel robot based on the waterbomb pattern. (c) Soft worm robot spired by the waterbomb pattern.

Even though this pattern is very well known, we still can consider our design a novel approach as no one has tried to used it as a pneumatic contractible soft actuator (as far as we know).

It should also be mentioned that we have introduced some alterations in the basic design. In order to improve the contraction ratio of the Magic Ball, we changed the pattern of the outer cells, transitioning from the waterbomb pattern to the Miura-Ori pattern, which is another well know auxetic pattern.

Furthermore, different configurations of the Magic Ball design can be created with a single sheet of paper depending on the number of cells in the design. In our case, we used a 28cm x 14cm paper sheet to create three basic designs: 4x8 cells, 6x12 cells and 8x16 cells, each square cell having a side length of 3.5cm, 2.33cm and 1.75cm respectively.

4. GEOMETRY VERIFICATION

When we selected the waterbomb geometry for our actuator, we knew that it could potentially act as a contraction actuator as it can transform from a tubular shape to a wheel shape when a force is applied axially (Fig. 19 (a)). However, we realized that the deformed shape obtained by pressurizing this geometry should be different from the one obtained when applying external forces. Therefore, we decided to fabricate a paper based prototype of our actuator to quantify the real contraction ratio for the different variations of the geometry. To do so, we got inspired by the article "Elastomeric Origami: Programable Paper-Elastomer Composites as Pneumatic Actuators"[54], where several pneumatic actuators are produced based on silicone and paper.

4.1. Elastomeric Origami

In this paper[54], Martinez *et al*. produced three different actuators based on silicone and paper or fabric and several variations of these actuators. We could have included them in the State of the Art chapter, but we decided to leave them apart because of their specific characteristics. The firsts actuator is a bending actuator similar to the ones described before. The second actuator is a linear contractor, obtained by embedding a sheet of a lengthwise trimmed paper into a tube of silicone. When the actuator is pressurized the rubber tends to expand but the encapsulated paper limits this expansion allowing the actuator to contract upon inflation. Despite being interesting actuators, we can't use any of the provided information because these actuators rely on the expansion of the silicone to operate. However, the design and operation of the third actuator is especially interesting to us.

The last pneumatic actuator they propose is an origami based linear extensor. In this case, a sheet of paper with the specific origami geometry is covered with silicone. Unlike the other two cases, the expansion movement is not achieved by the interaction between the paper and the silicon, but only because of the rearranging properties of the paper surface. The main purpose of coating the paper with the silicone is firstly, to seal the actuator so it is airtight and secondly, to define a resting contracted position for the actuator so it recovers the original configuration when the pressurized air is removed

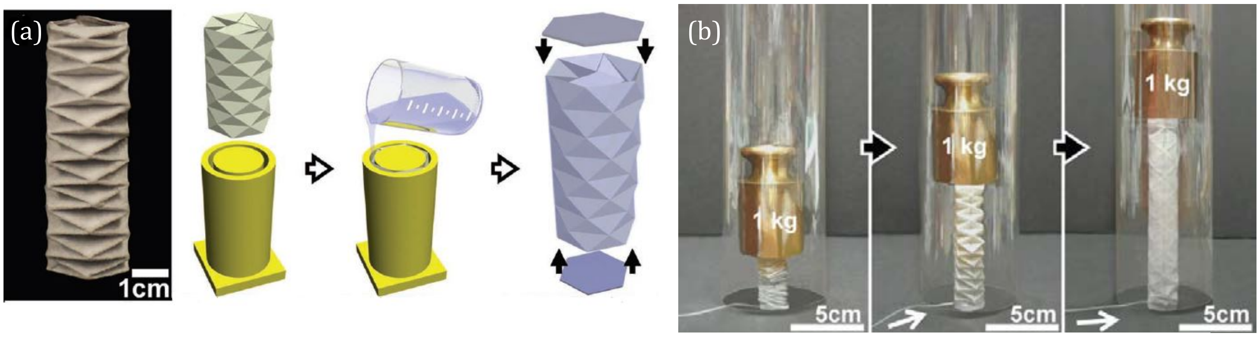

Fig. 20 Origami-based linear extensor. (a) Process of fabrication (b) Actuator lifting 1kg to maximum extension.

To fabricate this actuator, the base origami structure is folded to create the hinge pattern. Then it is unfolded and placed into a cylindrical mold, being then covered with Smooth-on Ecoflex 00-30 Silicone and degassed at 36 Tor for 3 minutes. Once the paper is soaked with liquid silicone, it is partially cured at 100ºC for 1 minute, holding it in a vertical position to obtain an even coat. When the silicone is hard enough to manipulate, the structure is folded, held in place using paper clips and cured for 30 minutes at 60ºC. Finally, two paper caps are glued in the extremes using the same silicone to create a sealed chamber.

This 8.3g actuator can lift 1kg (more than 120 times its weight) to its full extension being pressurized at 238mbar.

4.2. Prototype Fabrication Process

Given the similitudes between the actuator produced in the mentioned paper and our own actuator, we decided to apply their production process to our own actuator. However, we have found several obstacles that have lead us to modify this production method to fulfill our own needs.

Originally, we used the Smooth-On OOMOO 30 silicone to coat the paper although we quickly realized that this silicone was not a good choice for our prototype. The liquid silicone tended to accumulate in the pattern valleys, while only coating the top hinges with a very thin layer of silicone. When the actuator was pressurized, it radially expanded. The thick layer of silicone deposited on the pattern valleys exerted too much force in the thin top hinges and this, combined with the low elongation at break point of this silicone (250% of the original length), teared the silicone on the top hinges.

This problem was solved by using a different silicon, the Smooth-On Ecoflex 00-30. This silicon is actually the one used in the original paper. It has the same shore hardness than the previous one (Shore A 30) but lower viscosity (3000cps) and a considerably higher elongation at break point (900% of the original length). When it is applied to the paper surface it forms a thin and even coat that doesn't break when the actuator is pressurized.

It must be mentioned that, in the original paper, the paper was coated in both sides with silicone. In our case, we realized that this was not feasible. First and foremost, our actuator is not sealed in the ends by a paper cap. In our case, the free edges have to be folded and glued together in order to seal the actuator. This leaves a small entry where a 1/8" hose barb adapter is introduced and held in place. This hose barb adapter is used to connect the tube that will feed the pressurized air. If the actuator is coated on both sides with silicone, it becomes hard to glue the edges together and the hose barb adapter. The Ecoflex silicone is too weak to act as a glue between the edges and it can't hold the hose barb adapter when it is pressurized. Furthermore, the glues we used didn't stick well on the silicones. Therefore, the actuator's edges must be glued together and the hose barb adapter held in place before applying the silicone coat and thus, this makes it impossible to cover the actuator's insides with silicone. Furthermore, the inner silicone coat doesn't allow the actuator to reach its fully elongated state.

The selection of the glue used to glue the actuator's edges and the hose barb adapter was also problematic. We originally used Loctite Super Glue but, when the actuator was pressurized, the glue tended to stick to the hose barb adapter but separate from the paper, breaking the sealed compartment. We also tried the J-B Weld Plastic Bonder with similar results. After trying different glues, we figured out that the best way to keep the hose barb adapter in place was using a hot glue gun. The glue from the hot glue gun sticks well both to the paper and the hose barb adapter, allowing to create a more resistant and airtight actuator.

However, after some contraction cycles, the glue can separate slightly from the paper or the hose barb adapter, impairing the airtightness of the device. That is why we reinforced the end caps with a layer the OOMOO 30 silicone.

After all these considerations, the prototype production process can be summarized in the following steps:

1. The first step consists in folding a 28cm x 14cm piece of paper or cardboard into the desired waterbomb pattern. This process can take a considerable amount time due to its complexity. The simplest geometry (4x8 cells) can be folded in approximately 20 minutes while the 6x12 and 8x16 cells geometries may take 40 and 60 minutes respectively.
2. Once the flat paper has been folded into the desired geometry, the surface needs to be closed into a tubular geometry. To do so, a paper based tape is used so the obtained hinge had similar properties than the paper.
3. The next required step consists in closing the ends of the tubular geometry to create an enclosed volume. To do so, the external contiguous edges are glued together using a hot glue gun. Then, a 1/8" hose barb adapter was secured in both actuator's extremes using again the hot glue gun.

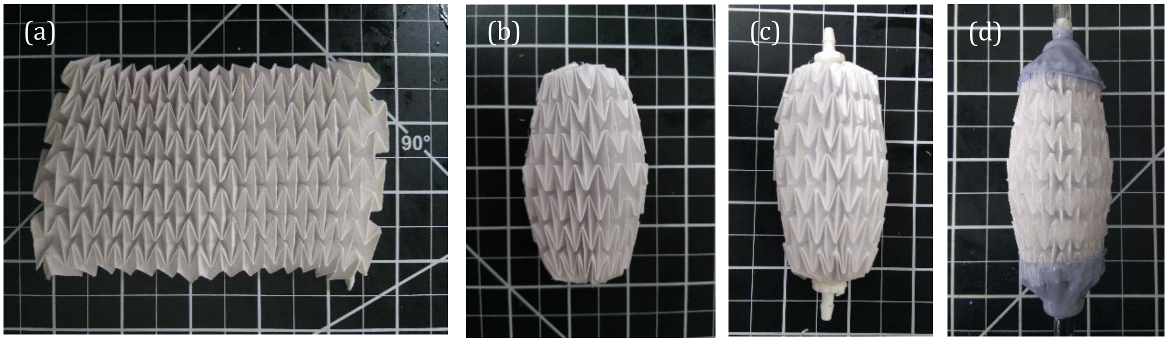

Fig. 21 Waterbomb actuator prototype fabrication process. (a) 8x16 waterbomb pattern. (b) "Magic ball" configuration, obtained thanks to a paper based tape. (c) Prototype with the edges glued together and the 1/8" barb hose adapter held in place. (d) Complete prototype covered with Smooth-On Ecoflex 00-30 and reinforced in the ends with Ecoflex OOMOO 30.

4. Then, the actuator is covered with a thin layer of Smooth-On Ecoflex 00-30 silicone. To apply this layer, the actuator must have a semi-contracted configuration so the silicone doesn't accumulate into the pattern's valleys. Then, the silicone is pre-cured during 5 minutes at 60ºC, rotating it every 30 seconds to obtain an even coat. When the silicone becomes hard enough, the actuator is hold into the fully elongated configuration using cable zip ties and cured for 30 minutes at 60ºC. After this process, the actuator's resting position is close to the fully extended configuration.
5. The last step consists in reinforcing the end caps with Smooth-On OOMOO 30 to avoid air leaks. This layer of silicone is cured for 60 minutes at 60ºC, while keeping the actuator is the full elongated configuration.

Using this procedure, we build 3 different configurations, (4x8 cells, 6x12 cells and 8x16 cells, each square cell having a side length of 3.5cm, 2.33cm and 1.75cm respectively) out of two different 14cm x 28cm sheets of paper (regular 75g/m^2 paper and a thicker 176 g/m^2 cardboard). A total of 6 waterbomb-based actuators.

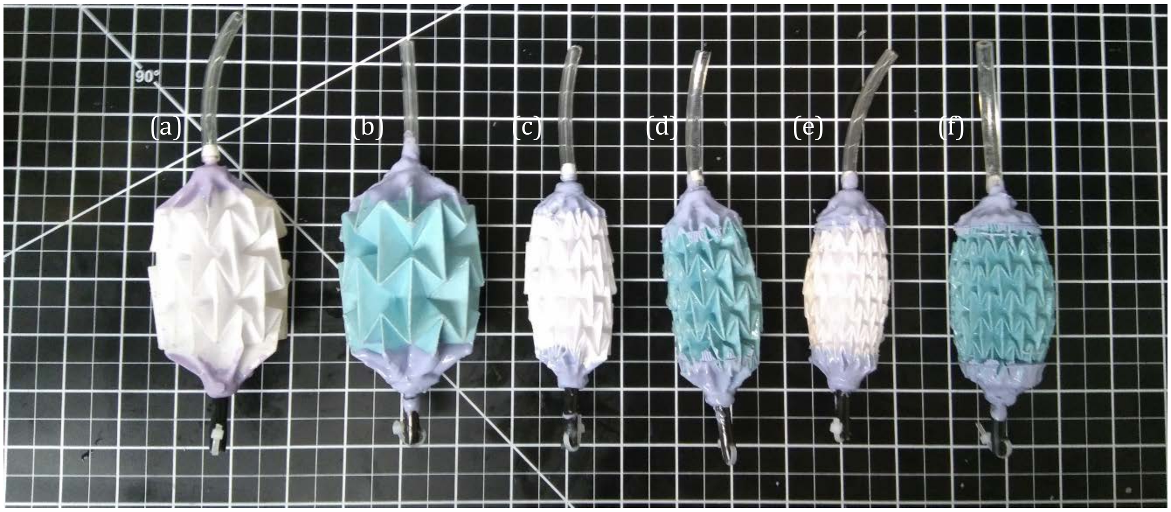

Fig. 22 6 different waterbomb-based prototype actuators: (a) 4x8 in paper, (b) 4x8 in cardboard, (c) 6x12 in paper, (d) 6x12 in cardboard, (e) 8x16 in paper and (f) 8x16 in cardboard.

4.3. Testing Bench

The actuators produced by the method explained in the previous section needed to be tested. However, we didn't have access to any equipment that could test our actuators. Therefore, we decided to build a simple test bench to fulfill our needs.

The main purpose of this testing station is to quantify the contraction ratio and the inner pressure of the prototypes upon inflation. This apparatus is shown in Fig. 23.

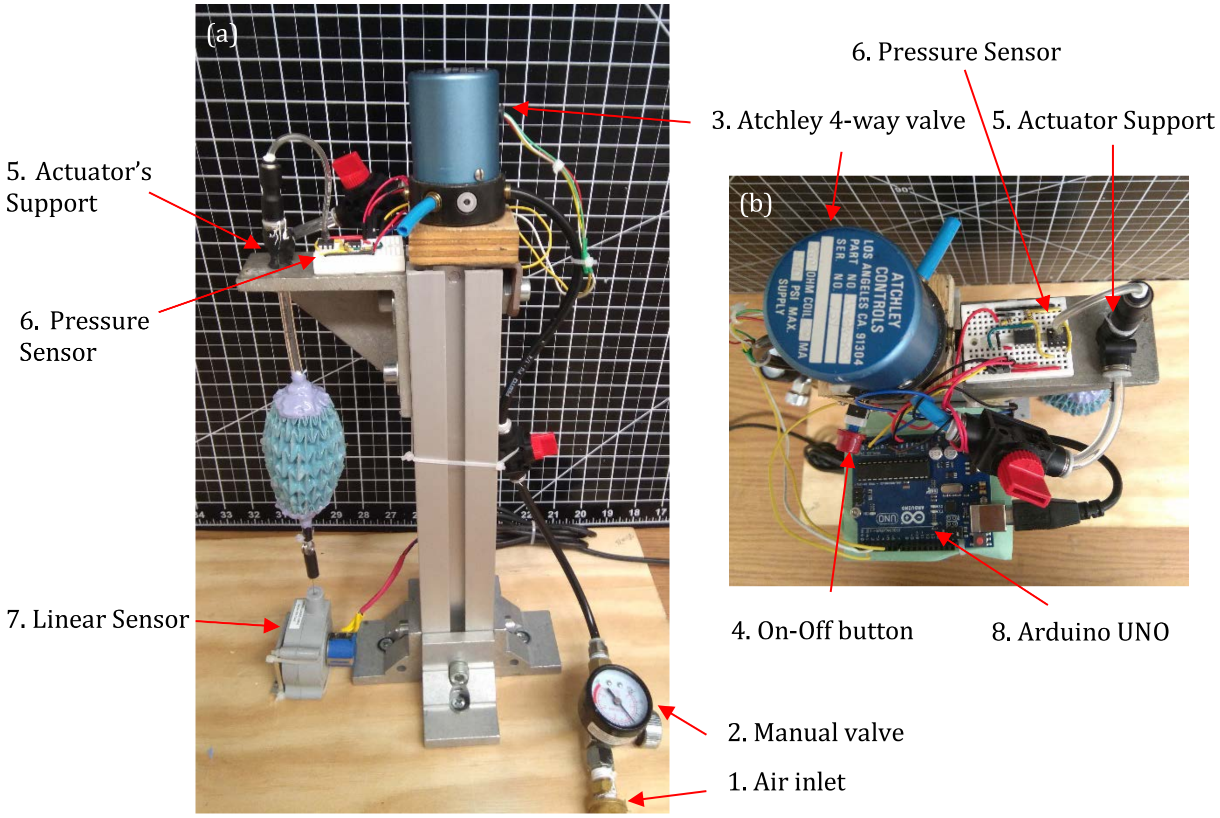

Fig. 23 Prototype Testing bench. (a) Frontal view. (b) Superior view

This testing bench consists mainly of a straight aluminum chassis which stands vertically upon a wood base. The chassis has attached an L-shaped metal piece where the actuators can be held perpendicular to the base. We decided to build the main chassis like this so we can apply different loads to the actuator by hanging weights at the actuator's lower end.

The inlet air flow (1) is regulated by a manual valve (2). This is necessary because the inlet pressure and flow are considerably high (60psi or 4atm.).

The inlet air flow is connected to the actuator through an Atchley 4-way valve. We decided to use this valve because it can be controlled directly with an Arduino board (8) and makes the design simpler (in case of using 2-way valves, we should use two valves instead of one).

We added an On-Off button (4) that switches the 4-way valve mode, so the actuator can be both pressurized and depressurized. This could be done through software. However, as the maximum pressures and contraction ratios for every actuator are still unknown, we needed to switch manually the valve, from pressurizing mode to exhaust, once the actuator reached the fully contracted position.

In order to record the actuator's pressure, a MPS20N0040D pressure sensor (6) was used. We chose this sensor because it is cheap and its pressure gauge range goes from 0 to 5.8 psi (or 40kPa), which fits our needs. This sensor is connected to the actuator's support (5) so it is located as close as possible to the actuator for an optimal sensing.

It is important to mention that this pressure sensor can't be directly read by the Arduino UNO board. This sensor's output are two signals around 2.5V which difference is proportional to the input pressure and ranges between 50mV and 100mV. A LM58N operational amplifier is used to subtract the pressure sensor outputs and amplify the resulting signal so it can be plugged into the Arduino board.

Finally, the contraction of the actuator is read through a Celesco SP1-25 linear sensor (7). This compact stringpot provides an output signal (0-5V) which is proportional to the cable's elongation (0-635mm). Although the resolution of the sensor is essentially infinite, the Arduino's can only split a 0-5V signal into 1024 (10 bits analog input port), having a resolution of 0.62mm. Considering that our actuators are around 100mm long, this resolution is not good enough. Therefore, we used a special library which allows us to increase the input port resolution from 10 bits to 12, having then a resolution of 0.15mm. It is important to mention that this sensor applies a force of 2N.

All the information provided by the sensors is managed by the Arduino UNO board and sent to a PC through the standard serial port

4.4.Test and Results

The prototype actuators produced in section 4.2 have been tested using the bench introduced in section 4.3.

In the fists test, we wanted to identify the prototypes maximum contraction ratios as well as to their general behavior.

To do so, we connected the actuators in the testing bench without any extra load. Therefore, the only load applied to the actuator is the 2N produced by the linear sensor. Furthermore, in order to test all the actuators under the same conditions, we fixed the airflow to 75cm^3/s using the manual valve attached to the air inlet.

We plotted the evolution of both the contraction and pressure among time to obtain the maximum contraction ratios and the inflation and deflation times. We also plotted the relative contraction against the inner pressure in order to identify the minimum pressure required for full compression. All these plots are attached in Appendix A.

The results obtained from testing all 6 actuators under these conditions are summarized in Fig. 24.

2N - Test results								
Pattern	Base material	Length[1] (mm)	Weight (g)	Contraction (mm)	Contraction (%)	Inflation time (s)	Deflation time (s)	Pressure[2] (Pa)
4 x 8	Paper	96.07	24.78	2.057	2.141	5.797	-	1.455
	Cardboard	99.24	27.81	7.122	7.177	6.617	-	5.523
6 x 12	Paper	90.24	24.34	9.496	10.523	2.554	14.420	1.489
	Cardboard	95.22	27.72	9.655	10.140	2.656	17.026	1.682
8 x 16	Paper	88.52	24.4	9.813	11.086	2.814	5.365	3.027
	Cardboard	92.84	28.58	11.555	12.446	2.971	6.460	3.640

Fig. 24 Results from testing all the prototype actuators shown in Fig. 22 under a 2N load and a 75cm^3/s airflow.
(1) The length in measured in the resting position form one hose barb adapter base to the other one.
(2) This pressure corresponds to the minimum pressure required to achieve maximum contraction.

First, we tested the 4x8 prototypes. The results are shown in *Fig. 54* and *Fig. 55*.

The blue line shows the evolution of both the absolute (mm) and relative (%) contraction ratios among time while the red line show the evolution of the inner pressure in time.

This data corresponds only to the inflation process. It can be observed that, while the pressure increases during the whole inflation process, the contraction ratio increases at the beginning and then starts decreasing. This is due to the geometry of this configuration (4x8). When the actuator starts inflating it keeps a spherical shape but there is a moment when in transitions to a cylindrical shape. When this happens, the structure expands instead of contracting. Therefore, we concluded that this specific configuration (4x8) is not appropriate for a contraction device and we will not test it under other loads.

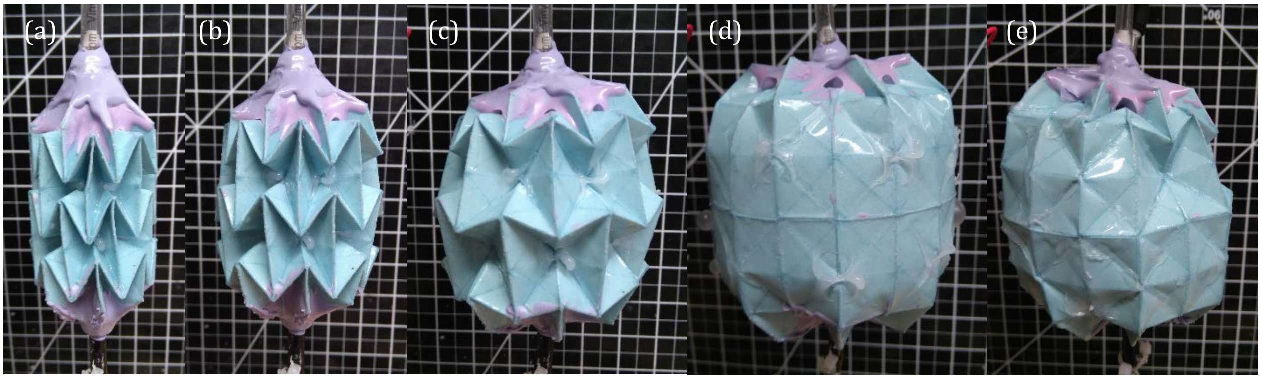

Fig. 25 Waterbomb buckling effect (a) Resting position (b) Inflation (contraction) (c) Inflation (expansion) (d) cylindrical fully inflated shape (e) Buckling effect. The actuator is not able to recover its original shape because the cell try to reach the alternative stable position by folding outwards.

Furthermore, we were not able to plot the deflation process because when the actuator takes the cylindrical form, the hourglass shaped cells invert, so the original shape cannot be recovered. This happens because the waterbomb pattern is a bistable structure. One of the functions of the silicone coat is to force the structure to fold into the desired stable configuration. However, if the pattern is fully unfolded it may not be able to recover the original stable position and transitions to the undesired one.

Also, while the cardboard structure remains always in the contraction scale, the paper based structure expands more than the original length. This happened because during the curing process, the paper structure wasn't held into the full extended configuration so the resting position of the actuator is semicontracted. We carefully cured all the other actuators to avoid this problem and optimize the contraction ratios.

Once we discarded the 4x8 structures, we proceeded by testing the 6x12 and 8x16 cell structures. The results are shown in the following figures.

The results shown in Fig. 56, Fig. 57, Fig. 59 and Fig. 58 prove that both configurations (6x12 and 8x16) could be potentially used as pneumatic contraction actuators. The paper and carboard based 6x12 configuration contracted 9.496mm and 9.655mm respectively (10.532% and 10.139% of their original lengths) while the 8x16 equivalents contracted 9.813mm and 11.56mm (11.086% and 12.45% of their original length). The 8x16 configuration seems to achieve slightly better contractions results both in absolute and relative terms.

It must be said that this contraction ratios are limited by the prototypes defects. There are small leaks that compromise the actuators ability to fully contract. Furthermore, the hose barb adapters are held in place by elastomeric materials so, when a load is applied the materials that joins them to the actuator stretch. If the actuators were completely airtight and the end caps properly held in place, the contraction ratios should improve. However, we don't think that the contraction ratio would never surpass a 20% of the actuator's length.

Both waterbomb configurations seem to behave very similarly. However, it can be observed that the time required to deflate the actuator once the airflow is interrupted is considerably higher in the 6x12 case. This may be related with the fact that the 6x12 configuration requires more air volume to fully inflate.

It also can be observed how the pressure curves are very similar. The inner pressure rises quickly when the valve is opened but the slope tends to decrease while inflating. When the actuators are near the maximum contraction ratio the pressure slope increases again.

The results shown in Fig. 56, Fig. 57, Fig. 59 and Fig. 58 could lead us to believe that the cardboard actuators require considerable more pressure to operate than the paper ones.

However, if we plot the inner pressure versus the relative contraction (Fig. 60 and Fig. 61) we can see that the resulting curves are very alike, only differing when on actuator contracts more than the other one.

The pressures required for full contraction in the 6x12 case round the 1.5Pa while in the 8x16 case is around 3Pa. This may be related with the number of hinges that have to be unfolded in order to contract. In any case, the required pressures are extremely low, which proves that this actuator could be used in portable applications.

It should be mentioned that Fig. 60 and Fig. 61 show that our actuators have some hysteresis. However, it is important to highlight that this results are obtained from transitory states. The pressure is recorded while inflating and deflating. If this recording process was done for stationary states, we are confident that the obtained hysteresis would be reduced. Furthermore, it is also important to notice that the pressure sensor is not located inside the actuator and this can also affect these results.

We repeated these tests under a 4N and 7N loads and an airflow of 90cm^3/s in both cases.

For the 4N tests we only tested the 6x12 and 8x16 configurations because, as we already said, the first set of tests proved that the 4x8 cell configuration can't be used as a pneumatic muscle. All the plots result of these experiments are attached in Appendix B and the results are summarized in Fig. 26.

4N - Test results								
Pattern	Base material	Length[1] (mm)	Weight (g)	Contraction (mm)	Contraction (%)	Inflation time (s)	Deflation time (s)	Pressure[2] (Pa)
6 x 12	Paper	90.24	24.34	5.856	6.489	1.928	4.324	2.53
	Cardboard	95.22	27.72	7.439	7.812	2.435	6.490	1.779
8 x 16	Paper	88.52	24.4	8.705	9.834	2.493	3.792	3.647
	Cardboard	92.84	28.58	9.813	10.639	3.036	6.335	4.199

Fig. 26 Results from testing the 6x16 and 8x16 configurations under a 4N load and a 90cm^3/s airflow.
(1) The length in measured in the resting position form one hose barb adapter base to the other one.
(2) This pressure corresponds to the minimum pressure required to achieve maximum contraction.

For the 7N tests we only tested the 8x16 configuration. The silicone of the 6x12 actuators tended to break under this load around the hose barb adapter. We think that the 8x16 configuration withstood this load better because the higher number of hinges allowed the silicone distribute the forces better.

All the plots result of these experiments are attached in Appendix C and the results are summarized in Fig. 27.

7N - Test results								
Pattern	Base material	Length[1] (mm)	Weight (g)	Contraction (mm)	Contraction (%)	Inflation time (s)	Deflation time (s)	Pressure[2] (Pa)
8 x 16	Paper	88.52	24.4	7.438	8.403	3.197	0.704	4.061
	Cardboard	92.84	28.58	9.180	9.952	3.749	1.720	4.682

Fig. 27 Results from testing 8x16 configuration under a 7N load and a $90cm^3/s$ airflow.

(1) The length in measured in the resting position form one hose barb adapter base to the other one.

(2) This pressure corresponds to the minimum pressure required to achieve maximum contraction.

All these results show that an increase in the load subjected to the actuator implies a decrease in the contraction ratio. It must be said, though, that these loss of contraction is in part influenced by the elasticity of the materials used to hold the hose barb adapters as well as the tubes and zip ties used to hold the actuator and the load in place.

On the other hand, an increase of the load also affects the inflation and deflation times. The inflation time tends to augment due to the fact that the actuator has to perform more work to lift the load while the deflation time decreases considerably as the actuator is able to expel the contained air quickly.

Finally, the pressure required to achieve the full contracted position also increases with the load.

All these conclusions can be easily observed in Fig. 28 and Fig. 29, where the contraction ratio, the pressure and the inflation and deflation time times are plotted for the different loads applied on the 8x16 configurations.

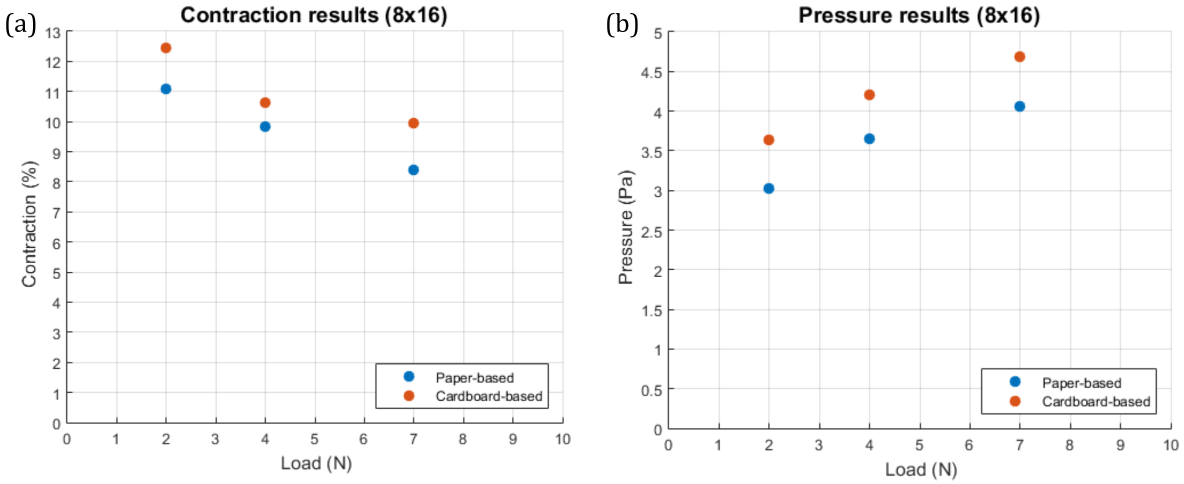

Fig. 28 Contraction and pressure results for the 8x16 configuration under 2, 4 and 7N loads.

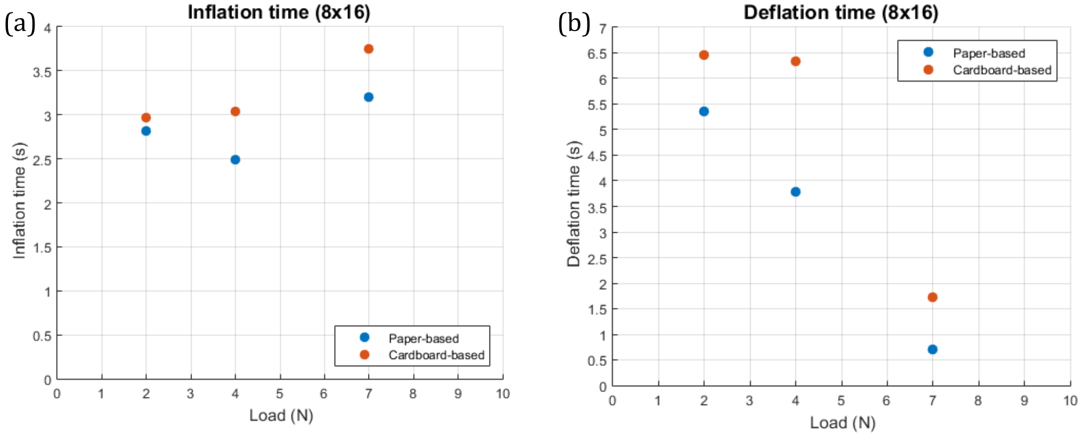

Fig. 29 Inflation and Deflation times for the 8x16 configuration under 2, 4 and 7N loads. The inflation results for the 2N case differ because the airflow is different than the other cases ($75m^3/s$ instead of $90m^3/s$).

These results also show that the paper-based configuration has a lower inflation and deflation times while the cardboard one achieves more contraction and inner pressures. It is important to mention that the cardboard structures resist better the bulking effect that the paper ones.

The main conclusions that can be extracted from these results are:

1. Both 6x12 and 8x16 waterbomb configurations can potentially be used as pneumatic artificial muscles while the 4x8 configuration is discarded.
2. The maximum of contraction ratio is low (10-15% of the original length) but the pressure required to operate the actuators is also very low (under 5Pa).
3. Thicker and more rigid membranes allow higher contraction ratios and reduce the bilking effect while thinner membranes are faster to operate.
4. The principal reason why the actuators failed is the end caps. The hose barb adapter separated from the paper and the silicone reinforcement failed. Therefore, a specific cap should be designed so it can be attached directly to the surface and can act as a force transmitter and air inlet. Furthermore, it would be interesting to embed the pressure sensor in one of these caps.

5. 3D PRINTING

The project's main challenge consists in 3D printing the tested geometry so it can be proven that a functional contraction soft actuator can be produced by these means. Before starting to work in the CAD design, we need to understand the features of the equipment that will be used.

5.1. 3D Printer features

Currently, there are not many 3D printers that can produce pieces with rigid and rubbery materials at the same time. This characteristic is mandatory for our purposes as our actuator can't be printed using only standard rigid materials.

Therefore, we used the Stratasys Objet260 Coneex3, a multi-material 3D printer that relies on a photopolymerizing process to produce the 3D models.

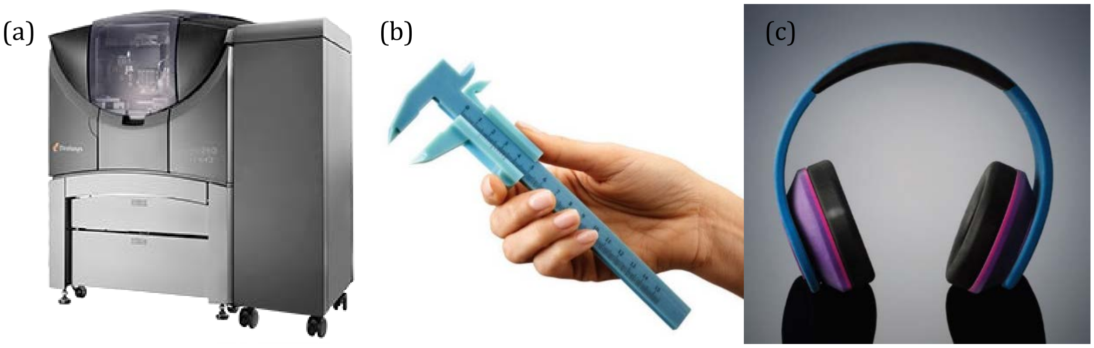

Fig. 30 Stratasys Objet260 Connex3 (a). (b) Caliper: example of this 3D printer's precision. (c) Headphones: example of piece printed with different materials. The pads are printed with a rubbery material while the main structure is printed with a rigid one.

As a multi-material 3D printer, this machine can produce parts with a wide range of mechanical, optical and thermal properties using a variety of different materials like Digital ABS, Simulated Polypropylene, Heat-resistant materials, Biocompatible polymers and Rubber. Furthermore, it also can produce mixtures from these basic materials creating hundreds of new Digital Materials, each one of them with specific mechanical properties. It must be said, though, that this printer can only use 3 different materials and a support material at the same time, which limits the amount of Digital materials that can be used in a single model.

As it has been said, this equipment relies on a photopolymerizing technology. Instead of melting a solid thread of plastic like other 3D printer technologies, this machine deposits little drops of liquid photopolymer and polymerizes them using UV light. This has several implications. In one hand, the fact the original material is in a liquid state favors the production of Digital Materials. On the other hand, as the material is deposited in a liquid state before the photopolymerization, a solid base is always required. This means that, unlike other 3D printers, this one can't create hollow structures. This is not exactly true as the 3D printer designers introduced the support materials to solve this problem. This supports are soluble waxy materials that are meant to assist the printing process by filling the voids. Once the 3D printing process is done, the support material can be removed. It must be said, though, that the support material can be hard to remove completely, especially in the case of cavities.

The net build size this machine can print is 255x252x200mm. Furthermore, it has a very high resolution: 600x600x1600 dpi. However, the resolution in the z axis is cut in half when using digital materials, so every layer of material is approximately 32 microns thick.

Finally, it must be mentioned that this 3D printer only prints in one direction. This usually doesn't carry any implications as the pieces have isotropic-like properties when they are thick enough. However, this affects considerably the mechanical properties of thin structures. Important anisotropies are produced, especially in the transversal direction of the printing, which is weaker at traction.

5.2. 4D Printing

Once we started working in the 3D printable design, we quickly realized that there were several complications that made hard to produce this actuator as a finished geometry.

The first and main problem was the complexity of the CAD design. The waterbomb pattern is not hard to reproduce in a CAD model if it is considered an infinite thin surface. However, it becomes harder when the thickness of the material is taken into account. Furthermore, it must be considered that different materials have to be used in the hinges (rubbery material) and the faces (rigid material). This means that the parts with different materials must be designed independently and then assembled, making the CAD design extremely complicated to produce.

There were also other problems, like the fact that printing directly the actuator would require large amounts of the waxy support material which would be hard to remove from the internal cavity. Furthermore, the production process would take several hours and the cost would be elevated.

Because all these reasons, we looked for alternative ways to produce the waterbomb actuator using the 3D printer so the complexity of the model, the printing time and the overall cost can be reduced.

After considering the process followed to produce the prototypes in section 4.2, we had a simple idea: is it possible to print a flat geometry that can be folded into the desired pattern?

We were aware of several technologies that allow flat origami-based structures to self-assemble into small robots[55–57]. There is also some research on flat pre-stressed sheets of polymer that can be folded by localized photoinduced stress relaxation[58,59].

This self-assembly concept has been also recently introduced in the 3D printing scope under the name of 4D Printing[60–62]. This term was first used in 2013 by MIT researcher Skylar Tibbits[63] and it refers to all the technologies that allows creating 3D structures using flat surfaces produced by 3D printers though self-assembling techniques. In these technologies, the 4th dimension is time as it refers to the ability of material objects to change form and function after they are produced through an external stimulus.

This technology fits our project as all these 4D printing technologies rely on the Stratasys Objet Connex 3D printers.

According to several sources[62,64], there are two main 4D printing technologies which are differentiated by the external stimulus used to transform the flat surface into the final structure.

5.2.1. Hydromechanically Activated 4D Printing:

This technology has been developed in collaboration between Stratasys and the MIT's Self-Assembly Lab, leaded by the 4D printing reference Skylar Tibbits. It relies on a PolyJet hydrophilic material that expands 150% when soaked in water.

The bending elements of this designs consist in a series of discs connected by a rubbery lamina of material. One of this lamina sides is covered with the mentioned hydrophilic material so, when the element absorbs water, it increases its volume making the hinge bend until the discs limit the bending action.[65,66]

This technology has been used in different publications to create different proofs of concept like single strand that self-folds into the letter MIT[66], a flat surface that self-folds into a closed cube[66] or a self-assembling octahedron[64].

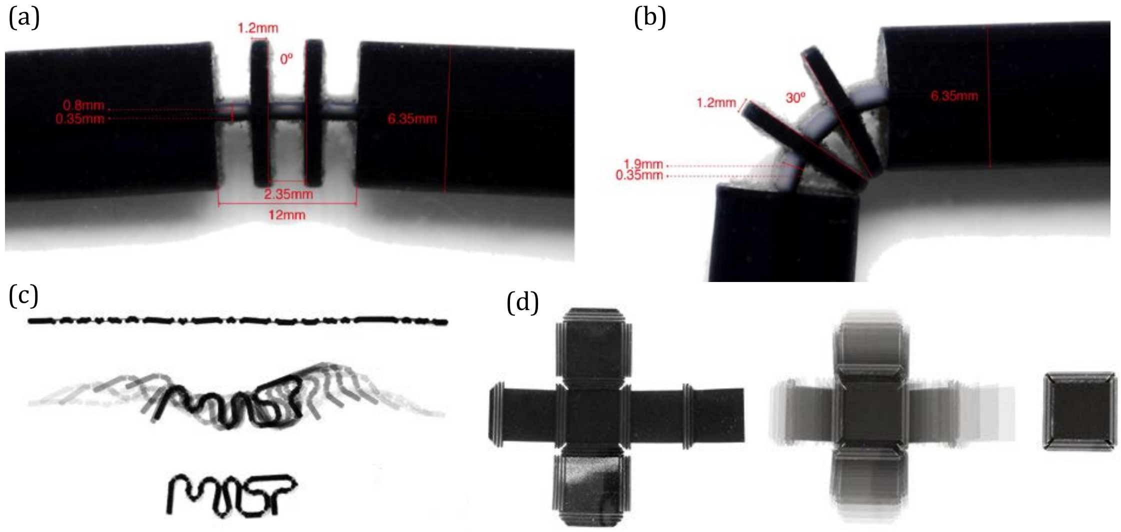

Fig. 31 Hydromechanically activated 4D Printing. (a) Basic hinge structure (b) Hinge deformation when soaked in water. (c) Single strand self-folding into the letters MIT. (d) Self-folding of a 3-dimenssional closed cube.

It must be mentioned that they also have developed a Software in collaboration with Autodesk called Project Cyborg. This software can simulate the 3D printed pieces so the behavior of the 4D printed structures can be predicted.

Unfortunately, both the hydrophilic material and the simulating software are not commercially available yet.

5.2.2. Thermomechanically Activated 4D Printing:

Researchers of the University of Colorado Boulder have created this 4D printing technique which relies on shape memory polymers (SMP)[67]. Rigid fibers with shape memory polymer characteristics (PolyJet Vero family materials) are embedded asymmetrically in an elastomeric matrix during the 3D printing process. Then, the hinge is heated, stretched and cooled, activating the shape memory properties of the embedded SMP. The difference of contractions between the activated SMP and the rubbery matrix makes the hinge bend. Therefore, these structures are also termed Printed Active Composites (PACs).

This technique has been used to fabricate different examples, like a self-assembling pyramid[67], a self-assembling cube[67,68] or even an origami airplane[67]. A variation of this technic has been also used to develop a sequentially activated shape changing geometry[69].

It is important to mention that researchers have reported important time savings using this technique[62]. A 20mm per side hollow cube with 1mm thickness was produced by 4D and 3D printing. The first one toke 10 minutes to be printed while the second one more than 3 hours.

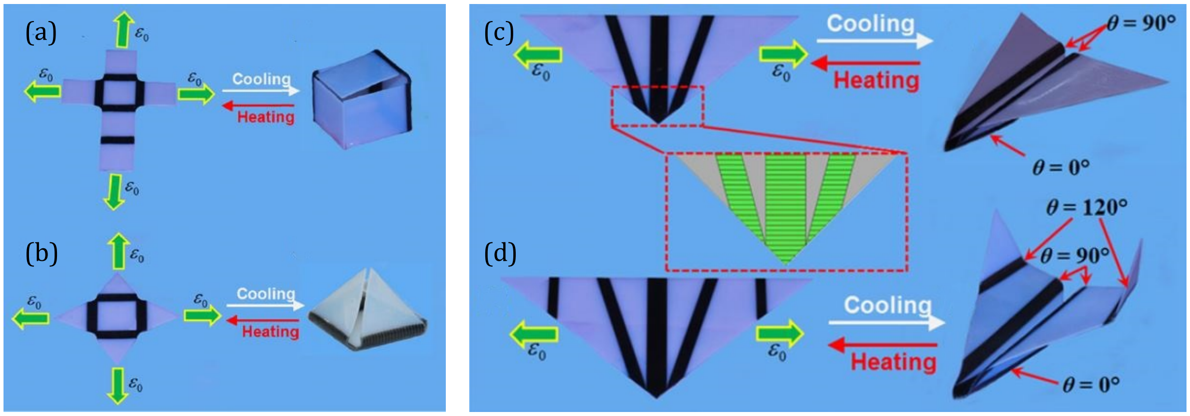

Fig. 32 Thermomechanically activated 4D Printing. (a) Self-folding cube, (b) Self-folding pyramid, (c) and (d) self-folding origami airplanes.

Both technologies could be potentially used to produce our desired geometry. However, due to the impossibility to use the hydro-mechanically activated 4D printing concept as the hydrophilic material is not commercially available, we decided to proceed using the thermomechanically activated 4D printing concept.

5.3. Active Origami

As a starting point, we based our design in the paper "Active Origami by 4D Printing"[67] by Ge *et al*.

This publication settles the bases for thermomechanically activated 4D printing by introducing a way to produce flat structures with a Stratasys Objet Connex 3D printer that can be thermomechanically programmed to self-fold into a desired configuration.

This flat structures consist in rigid panels connected by a Printed Active Composite(PAC) lamina, as shown in Fig. 33 (a). At the same time, the PAC lamina consists in a series of Shape Memory Polymer (SMP) fibers embedded in an elastomeric matrix. These SMP fibers are located asymmetrically respect the horizontal symmetry plane in order to produce the bending action when the hinge is thermomechanically activated.

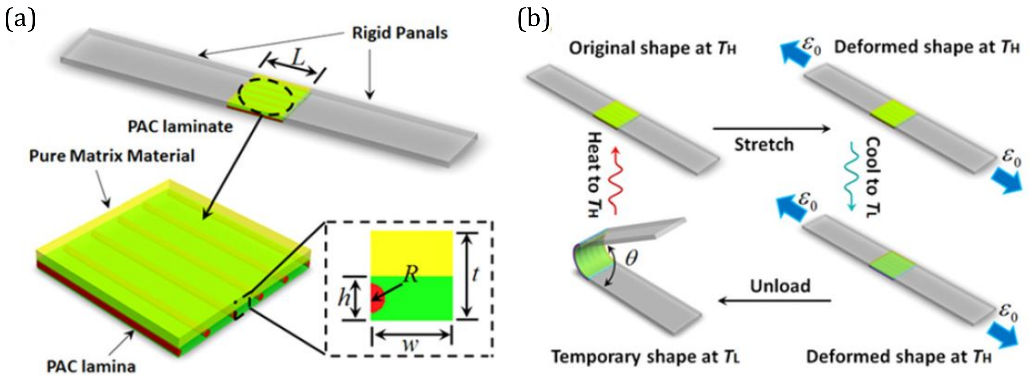

Fig. 33 Thermomechanically activated 4D Printing (a) PAC lamina structure. (b) Thermomechanical activation process.

Before explaining the PACs 4D printing activation process, we need to introduce the Shape Memory Polymer (SMP) concept. SMPs are polymeric smart materials that exhibit the Shape Memory Effect (SME). This means that they can change its original (permanent) shape into a deformed shape (temporary shape) induced by an external stimulus. They can also revert this effect through a stimulus recovering then the original configuration.

These SMP fibers present a semi-crystalline or "glassy" atomic configuration at regular room temperature. When the material is heated over a specific temperature known as glass-transition temperature (T_g) the atomic structure switches from the semi-crystalline structure into a more viscous or rubbery state. In this new state, the material can be easily deformed into a new shape. If the material is held in a deformed shape when cooling it down under its T_g, it will switch to a semi-crystalline atomic structure again, but this structure will differ from the original as it accommodates to the deformed shape, creating then a new temporary shape. However, if this deformed fiber is heated and cooled again without applying and external force, it will recover its original permanent shape.

The SME properties, like the glass-transition temperature (T_g) can be obtained by testing the material with a Dynamic Mechanical Analysis (DMA) machine. The storage modulus and tanδ are measured for different temperatures when performing a uniaxial tensile test. In this publication[67], this procedure was applied to obtain T_g for both the fiber and the elastomeric materials, as shown in *Fig. 34*.

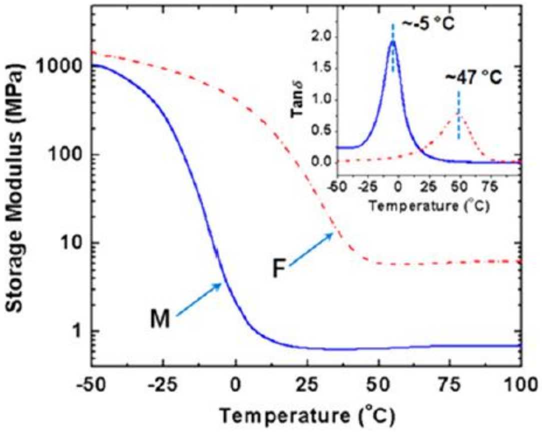

Fig. 34 Storage Modulus and tanδ vs Temperature for the PAC fiber and matrix material

In this publication, they indicate that the material used for the rubbery material is TangoBlack (T_g =-5ºC) while the SMP fiber are a combination of TangoBlack and a rigid plastic material known as VeroWhite (T_g=53ºC). This combination is a Digital Material which they refer as “Grey 60” (T_g=47ºC).

The thermomechanical programming process is shown in Fig. 33 (b). The PAC is heated over the glass-transition temperature (T_g). During this process, the fiber material switch from the semi-crystalline atomic configuration to the rubbery one while the matrix material doesn’t experiment any atomic structure modification as it is always working over its T_g. Then the sample is stretched a cooled down under the fiber’s T_g while keeping the sample in the deformed shape. This creates a stretched temporary shape for the fiber. When load is released, the matrix material tends to recover its original shape while the fibers try to keep the deformed shape, thus bending the hinge.

In this paper[67], Ge *et al*. tested 5 cross section geometries for 4 different hinge lengths (2.5, 5, 7.5 and 10mm). The best geometry (t=0.5mm; R=0.08mm; h=0.2mm; w=0.5mm) achieved hinge angles of approximately 120º, 55º, 20º and -10º for the 2.5, 5, 75 and 10 mm hinge case respectively when stretched up to 20% of the hinge length, as shown in *Fig. 35*.

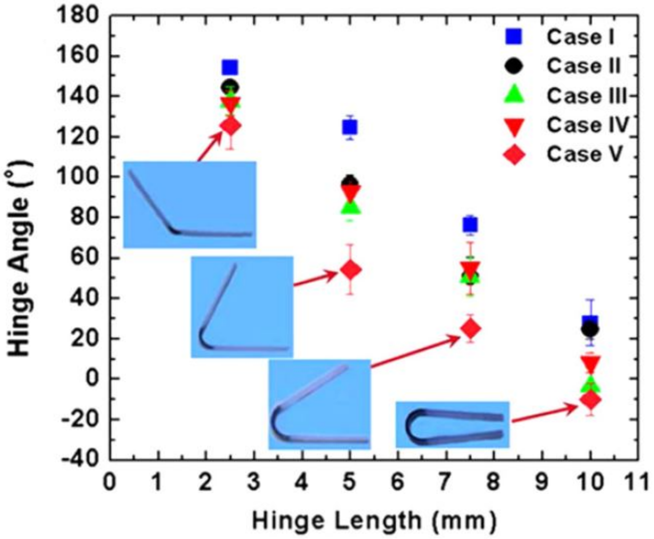

Fig. 35 Hinge angle vs hinge length for hinges with five different cross-section profiles pre-stretched by 20%.

5.4. Hinge Optimization

We decided to base our design in the results obtained by Ge *et al.* in the mentioned paper so we proposed using the case V configuration (t=0.5mm; R=0.08mm; h=0.2mm; w=0.5mm) as it presents the best results (*Fig. 35*). However, due to the dimensions of our designs (12cm x 24cm sheets), we couldn't use long hinges. In fact, we realized that our hinges should not be longer than 2.5mm.

Despite having the best performance of all geometries, case V only achieved a hinge angle of 120º. We considered that in our design, this angle should be at least 90º. Therefore, we decided to improve the performance of the 2.5mm hinge case by testing the influence of the materials, the fiber density, the fiber length and the hinge thickness.

To do so, we built a parametrized SolidWorks CAD model that allowed us creating different variations of the hinge geometry by changing the parameters.

These parameters are the hinge cross-section geometry parameters shown in Fig. 33 ("L", "h", "t", "w", and "d") and the parameters that define the rigid panels connected to the hinge (usually "L_sup" is kept as 10mm while "W_sup" is 15mm). Finally, another parameter is defined to specify the longitude of the fiber embedded in the rigid panel (used in the fiber length test).

For every sample, we used the same thermomechanical method to activate the self-folding process. The sample is heated by plunging it in water bath at 80ºC during 30 seconds. Then, the sample is stretched around a 30% of the hinge length and cooled in a 20ºC water bath during 30 seconds while keeping applied longitudinal stress. Finally, the stress is removed, revealing then the temporary shape. This new shape shouldn't be lost as the sample is not supposed to be heated over the fiber's T_g.

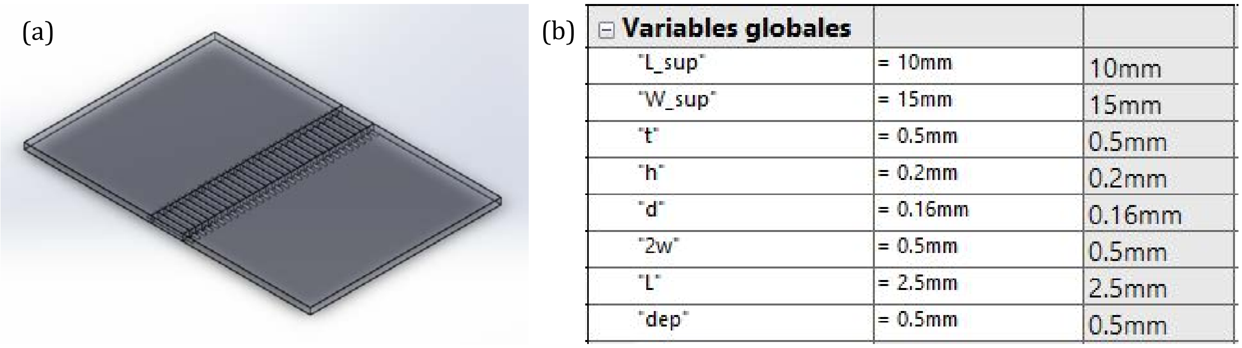

⊟ Variables globales		
"L_sup"	= 10mm	10mm
"W_sup"	= 15mm	15mm
"t"	= 0.5mm	0.5mm
"h"	= 0.2mm	0.2mm
"d"	= 0.16mm	0.16mm
"2w"	= 0.5mm	0.5mm
"L"	= 2.5mm	2.5mm
"dep"	= 0.5mm	0.5mm

Fig. 36 SolidWorks model (a) example of a test sample CAD design, (b) parameters used to change the sample geometry.

5.4.1. Material test:

Ge *et al.*[67] mentioned that they used TangoBlack as the rubbery matrix material while the SMP fibers were made of a digital material combination of TangoBlack and VeroWhite (actually, according to the Stratasys PolyJet material datasheet[70] this material should be named VeroWhitePlus-RGD835).

This misspell disconcerted us, as there is a rubbery material termed TangoBlack (FLX973) but there is another named TangoBlackPlus (FLX930) and their properties are slightly different, having TangoBlack more stiffness than TangoBlackPlus. We tried to get in touch with the authors to clarify which materials have they used. Unfortunately, we didn't get any response.

We only had VeroMagenta (RGD851) and TangoBlackPlus (FLX930) to our disposition.

Using VeroMagenta shouldn't be a problem as, according to the Stratasys PolyJet material datasheet[70], their physical properties are the same.

On the other hand, we have not found any reference to a "Grey60" material based on TangoBlack although, we found references[71] to a "Grey60" composed of TangoBlackPlus and VeroWhitePlus which technical code is DM8530, so we assumed that were using the correct material.

For every combination of a rigid and rubbery PolyJet materials there is an array of digital materials. These materials are grouped into two main categories: rigid and flexible. The rigid material code is always ended by 05, 10, 15, 20, 25 or 30, being the material finished in 05 the one with more concentration of rigid material while the one finished by 30 is the one with less rigid material in its composition. The same happens with the flexible materials, being their codification finished in 40, 50, 60, 70, 85 and 95, being this number Shore A Hardness associated to the digital material.

Fig. 37 shows the codification used for the digital materials combination of TangoBlackPlus and VeroWhitePlus and its VeroMagenta equivalent.

	TangoBlack+ (FLX980)	
Flexible	FLX9840-DM	FLX-MK-S40-DM
	FLX9850-DM	FLX-MK-S50-DM
	FLX9860-DM	FLX-MK-S60-DM
	FLX9870-DM	FLX-MK-S70-DM
	FLX9885-DM	FLX-MK-S85-DM
	FLX9895-DM	FLX-MK-S95-DM
Rigid	RGD8530-DM – “Gray60”	RGD-MK-K60-DM
	RGD8525-DM – “Gray50”	RGD-MK-K50-DM
	RGD8520-DM – “Gray40”	RGD-MK-K40-DM
	RGD8515-DM – “Gray30”	RGD-MK-K30-DM
	RGD8510-DM – “Gray20”	RGD-MK-K20-DM
	RGD8505-DM – “Gray10”	RGD-MK-K10-DM
	VeroWhite (RGD835)	**VeroMagenta (RGD851)**

Fig. 37 Digital material codification

As the material used for the fibers “Grey 60” is supposed to be the softest material in rigid spectrum, we decided to test the other more rigid combinations to see if the resulting hinge angle could be improved. We tested 6 samples, each of one used one of the rigid digital materials for the fibers. The rigid panels connected to the hinge were made of pure VeroMagenta while the elastomeric matrix was composed of TangoBlackPlus. The hinge length was set at 5mm.

The results are shown in Fig. 38.

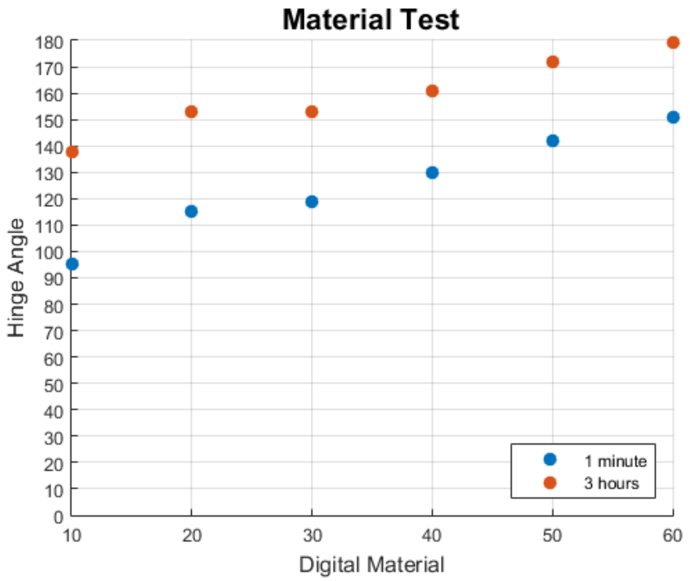

Fig. 38 Material Test. 5mm hinges thermomechanically activated with 20% strain. Digital materials are combination of TangoBlackPlus and VeroMagenta: RGD-MK-K10-DM, RGD-MK-K20-DM, RGD-MK-K30-DM, RGD-MK-K40-DM, RGD-MK-K50-DM and RGD-MK-K60-DM, being 10 the most rigid and 60 the softest.

The obtained results are surprising. According to the original source[67], a 5mm hinge embedded with “Grey 60” fibers should bend up to 60º (*Fig. 35*). This measurement is supposed to be done 1 minute after the thermomechanical process is applied as they consider that at that point the resulting hinge angle is stationary. However, our tests show that the equivalent of “Gray 60”, RGD-MK-K60-DM achieves an angle of ∼151º after 1 minute. Furthermore, this angle decreases with time, recovering the original shape after 3 hours, approximately.

On the other hand, we proved that more rigid fibers achieved higher bending angles. The hinges containing the RGD-MK-K10-DM fiber achieved an angle of 95º after one minute (closer to the 60º showed in the original source) although it lost around half of the achieved angle after 3 hours.

This results lead us to think that the actual material used as fibers in the original source was “Grey 10” instead of “Grey 60”.

Although the results are not as good as expected, we decided to use the material with the best SMP properties, the digital material RGD-MK-K10-DM, and try to optimize the hinge geometry parameters to increase the stationary hinge angle.

5.4.2. Fiber density test

In the original source, the distance between fibers (parameter “2w “) was kept constant at 1mm in all cases. We decided to test different samples with the Case V cross-section geometry but with reduced distance among fibers. In this case, we tested a total of 4 different samples with 2.5mm hinge length and RGD-MK-K10-DM as the fiber’s material. As in the previous case, the rigid panels connected to the hinge are made of pure VeroMagenta while the elastomeric matrix was composed of TangoBlackPlus. The tested distantness between fibers are 1mm, 0.75mm, 0.5mm and 0.25mm.

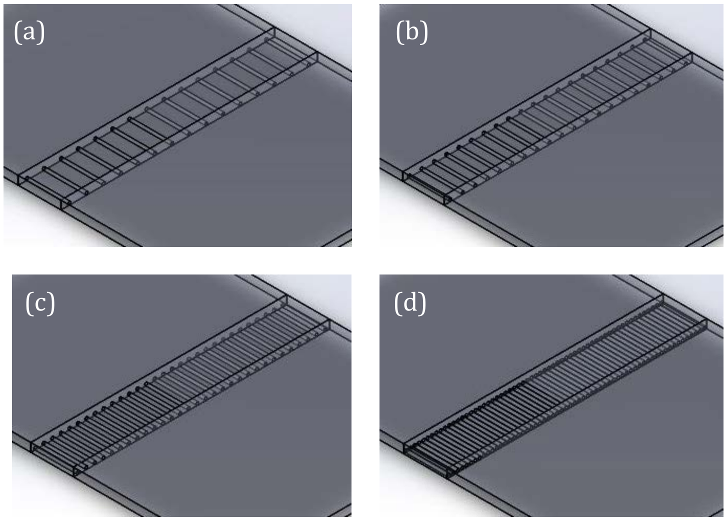

Fig. 39 CAD models details for the fiber density test. (a) 2w=1mm, (b) 2w=0.75mm, (c) 2w=0.5mm, (d) 2w=0.25mm

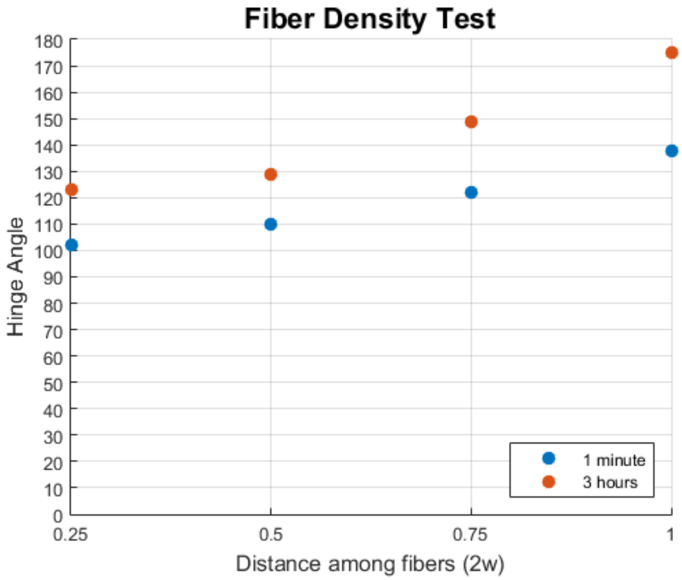

Fig. 40 Fiber density test. A total of 4 samples are tested, each one with a fiber separation of 2w= 1mm, 0.75mm, 0.5mm and 0.25mm.

Fig. 40 shows the results of these tests. The first important thing to notice is the positive impact that an increase of the fiber density has on the achieved hinge angle. This improvement does not only increase the achieved angle 1 minute after applying the thermomechanical process but also reduces considerably the angle lost after 3 hours.

It must be mentioned that, in the 2w=1mm case, the obtained results are worst that in the previous experiments because we reduced the hinge length from 5mm to 2.5mm. This was done because our waterbomb pattern require the shortest possible hinges.

5.4.3. Fiber length test

After proving the beneficial impact of increasing the fiber density, we wondered if we could be able to still improve the bent hinge angle. We realized that the hinge and the colliding panels were treated as independent parts. We decided to embed part of the fiber in rigid panels connected to the hinge, increasing then the total hinge length.

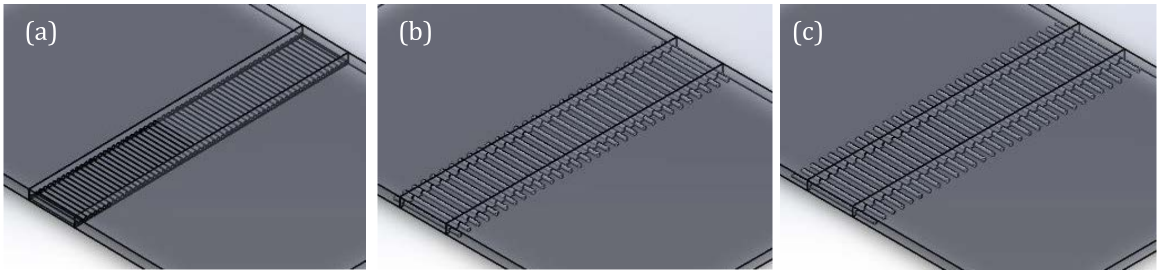

Fig. 41 CAD models details for the fiber length test. (a) Embedded 0mm in the rigid panels, (b) Embedded 0.5mm in the rigid panels (c) Embedded 1mm in the rigid panels.

We performed 3 different test, which geometry is shown in Fig. 41. We embedded part of the fiber in the rigid panels connected to the hinge. We tested a sample without the fibers embedded in the panels (0mm) and the 2 fiber with different fiber length embedded in the panels (0.5mm and 1mm).

In this case, we used TangoBlackPlus for the elastomeric matrix, RGD-MK-K10-DM for the fibers and two different materials for the panels: rigid Vero Magenta and the softest rigid digital material, RGD-MK-K60-DM. For this experiments, the fibers were separated half a millimeter (2w=0.5).

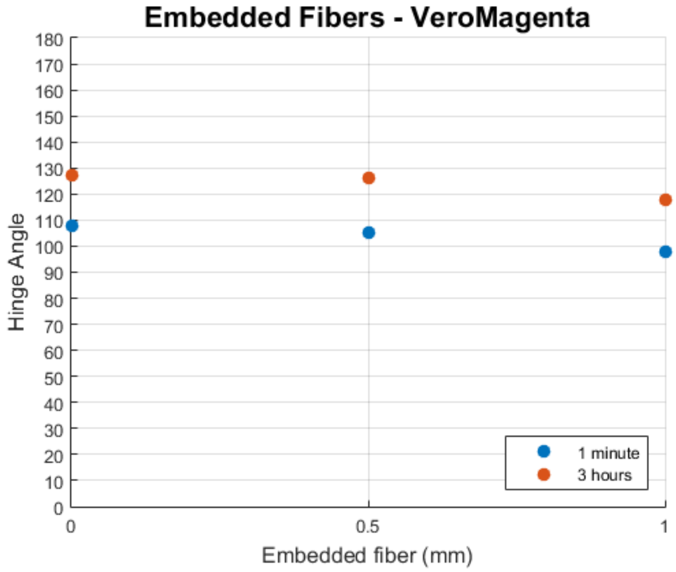

Fig. 43 Fiber length test using VeroMagenta for the rigid panels.

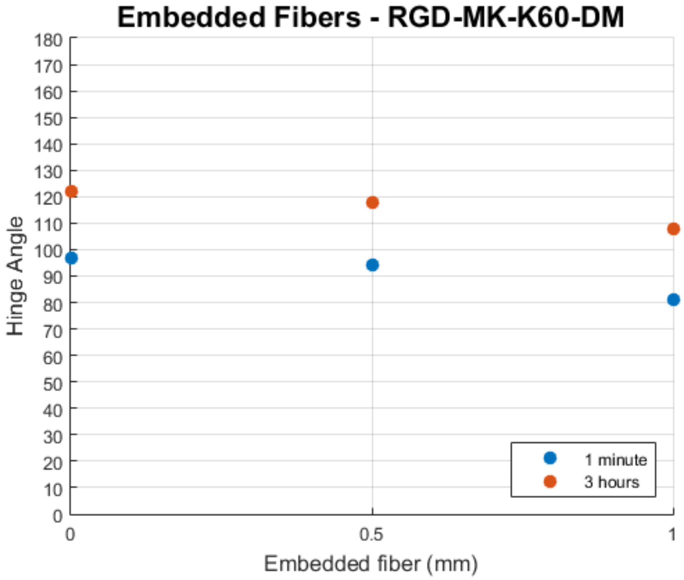

Fig. 42 Fiber length test using RGD-MK-K60-DM for the rigid panels.

These tests results (Fig. 43 and Fig. 42) show a slight increase in the achieved hinge angle after 3 hours when the fiber is embedded up to 1mm in the rigid panels (around 10-15º) while there is not a significant increase in the 0.5mm embedded case.

Furthermore, is interesting to see how the test performed with the softer material for the rigid lateral panels bent slightly more (~10º) than the ones made of pure VeroMagenta. This is a consequence of the rigid panels being slightly bent in the areas where the fibers are embedded.

5.4.4. Optimized hinge

After all these tests, we considered that the most appropriate hinge design for our pattern should consist in a basic case V cross-section with the following parameters: L=2.5mm; t=0.5mm; d=0.16mm; h=0.2mm; w=0.25mm and dep=1mm. This means that the 3D printed sheets must be 0.5mm thick and the hinge length 2.5mm. The fibers diameter must be 0.16mm and their center have to be placed 0.1mm from the hinge base. The fibers have to be separated 0.5mm between each other.

It should be mentioned that we chose a spacing between fibers of 0.5mm instead of 0.25 (which obtained better test results) because we were worried that too much rigid material would compromise the hinge ability to bend once the temporary shape is achieved.

We decided to use RGD-MK-K10-DM for the fibers, TangoBlackPlus for the elastomeric matrix and RGD-MK-K60-DM for the rigid sections of the pattern.

The selected design is able to maintain an angle of ~110º after 3 hours (which we consider stationary). This hinge stationary angle is not as good as the one we aimed for (90º at least). However, considering the difference in results that we got respect the original source we decided that should be enough for our purposes.

5.5. CAD Design

Once the hinge specifications for the 4D printed waterbomb pattern were chosen, we proceeded by creating the 3D CAD design for the flat structure.

Originally, we wanted to create the 8x16 cell pattern for a 12cm x 24 cm base sheet. However, the hinge length (2.5mm) makes it almost impossible as the remaining rigid surfaces (the triangles in the pattern) were too small. Furthermore, as the 3D printed sheet has a certain thickness (0.5mm), we needed to create soft nodes were the hinges come together to reduce stress concentration, reducing even more the rigid surfaces area.

Therefore, we decided to print the 6x12 cell pattern on a 12cm x 24cm sheet (this is the maximum dimensions than can be achieved as this 3D printer's tray is only 255x252mm^2).

The CAD design presented several challenges in different parts of the model. Therefore, we designed separately the basic cells, the outer edges and the two edges that must be bonded together to create a cylindrical closed surface.

It is important to consider that the CAD model must be built in several main parts, each one associated with the material that will be assigned during the 3D printing process. Therefore, at the end we only should have 3 SolidWorks parts that can be put together in an assembly file to create the final geometry. This pats are the fibers (RGD-MK-K10-DM), the elastomeric hinge matrix (TangoBlackPlus) and the rigid panels (RGD-MK-K60-DM)

5.5.1. Cell design

The basic cell geometry is the base of the CAD design as it is repeated in almost all the model's surface except in the outer rims.

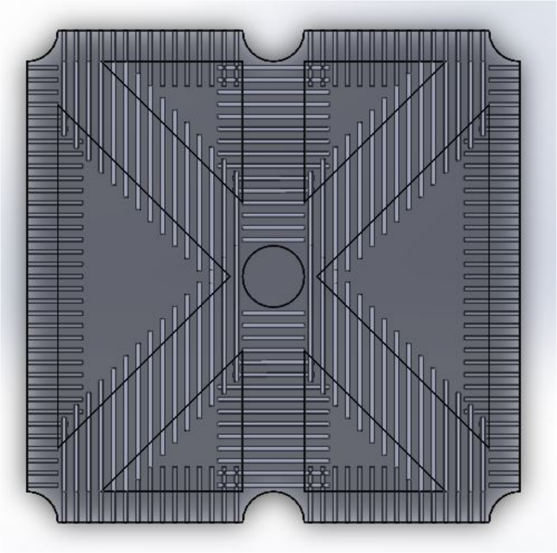

Fig. 44 Basic CAD cell design for the 4D printable 6x12 cells waterbomb pattern

This design (Fig. 44) consists in several triangles (rigid parts) surrounded by a frame that corresponds to the elastomeric matrix. Both the rigid triangles and the elastomeric frame have cylindrical holes specially located to accommodate the SMP fibers in place.

It is important to mention that not all the fibers are placed in the same plane. In the waterbomb cell design, all vertical and horizontal hinges have to bent in the same direction while the diagonal hinges must bend in the opposite direction. Therefore, the vertical and horizontal fibers are closer to the bottom while the ones corresponding to the diagonal hinges are closer to the top.

It must also be said that we chose to place the fibers corresponding to the diagonal hinges in the vertical direction instead of the hinge's perpendicular direction for space optimization purposes.

Finally, we left some pure elastomeric areas where the hinges come together to avoid stress concentrations.

5.5.2. Outer edge

The outer edge corresponds to the longer sides of the 12cm x24cm rectangular sheet. This sides have to be folded and glued together to close the cylindrical shape into a spherical shape. As it is shown in Fig. 45, every rhomboidal rigid panel must be glued to its contiguous panels by the longest edge. This closes the geometry and leaves two small entries where the hose barb adapters will be placed to seal the actuator.

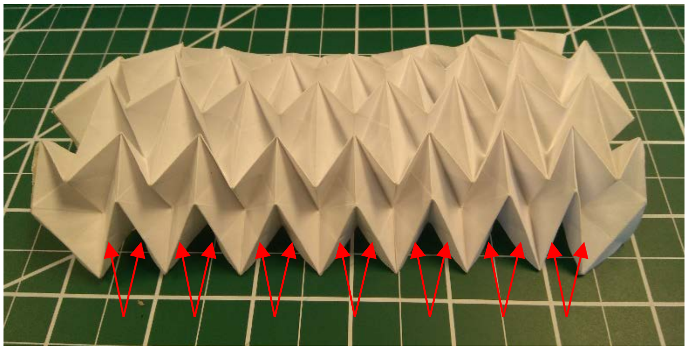

Fig. 45 Outer ridges for the paper-based waterbomb pattern. The pointed edges have to be glued together to seal the actuator. It can be seen how in this case, the rhomboidal panels are connected by two triangular panels which will be removed in the CAD design.

In our design, we have eliminated the small triangular panels that connect the rhomboidal ones so the long edges of the 12cm x24cm rectangular sheet are no longer straight but a zigzag line.

It should be mentioned that, as the rhomboidal panels must be glued by hand, we haven't reinforced the hinges that connect them because they don't need to be thermomechanically activated.

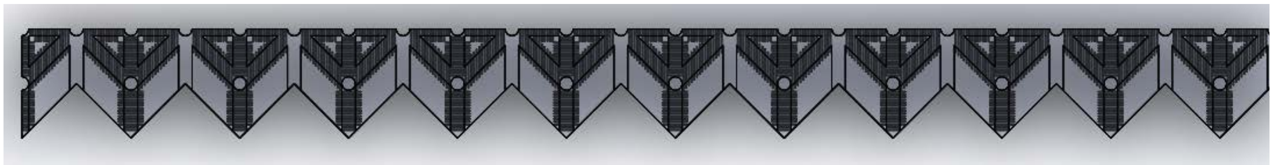

Fig. 46 Detail of the CAD zigzag design for the outer edges

5.5.3. Bonding edge

The other main problem we had to solve is how to close the flat 3D printed surface into a cylindrical surface. In this case, we couldn't use the paper-based tape like in the paper designs. We needed to create a stronger bond that makes the actuator air-tight but also preserves the SPM properties of that specific hinge.

The two short ends can't be glued directly together because of the small area that connects them (the sheet is only 0.5mm thick). Therefore, we came up with a design that overlaps the contiguous rigid panels and hinges in order to optimize the surface bonding area while maintaining the hinge properties. This design is shown in Fig. 47.

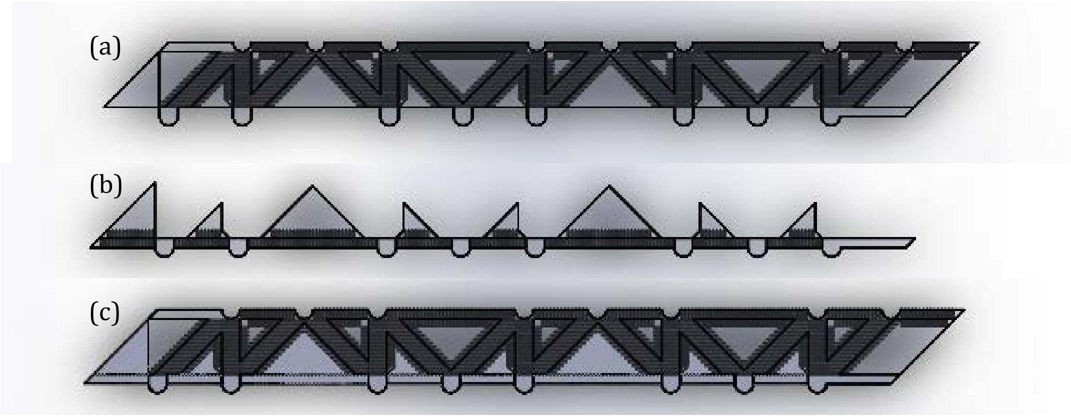

Fig. 47 CAD detail of the bonding edges (a) Rigth edge, (b) Left edge, (c) bounded edges

5.5.4. Full CAD design

All the mentioned elements are put together in a single CAD assembly composed of three SolidWorks parts: the rigid panels, the elastomeric matrix and the fibers. This final design is shown in Fig. 48.

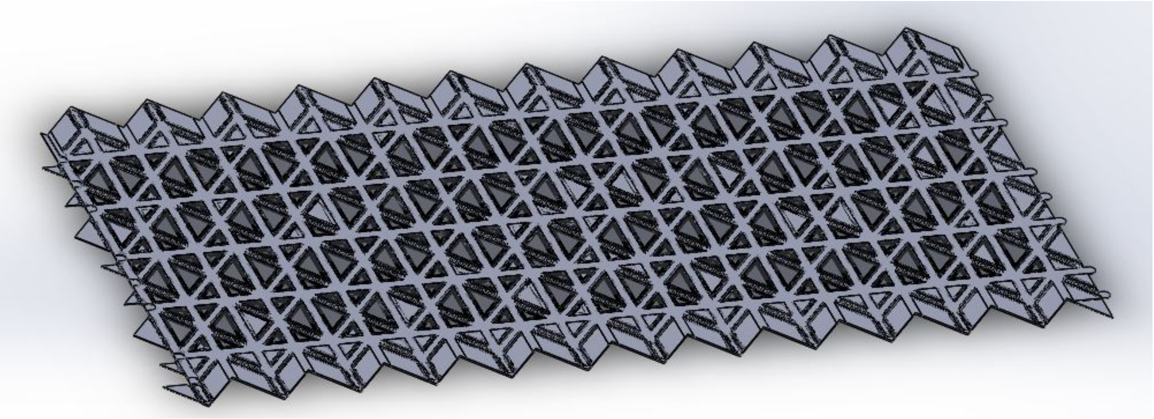

Fig. 48 CAD design for the 6x12 cell waterbomb pattern from a 12cm x 24cm base sheet.

5.6. Assembly

After producing the CAD model, we proceeded by 3D printing and assembling the actuator.

At the beginning, we intended to apply the thermomechanical activation process to the 3D printed flat sheet and then close and seal the folded geometry to create the actuator. However, we realized that it would be hard to stretch evenly all hinges due to the complexity of the pattern and the different orientation of fibers.

Therefore, we concluded that the best way to apply an even force to all hinges should be by sealing first the actuator and use pressurized air to exert the required force upon the hinges.

The assembling process can me summarized in the following steps:

1. We started by using the standard Stratasys software for the Objet260 Coneex3 to set all the required parameters, including the materials assigned to each part of the model. As the dimensions of the base sheet are approximately 12cm x 24cm and the tray area is 25.5cm x 25.2cm, we decided to 3D print two base sheets at the same time. The 3D printing process toke 29 minutes and it costed around 40USD. Once the base sheets were printed, the waxy base material had to be removed.

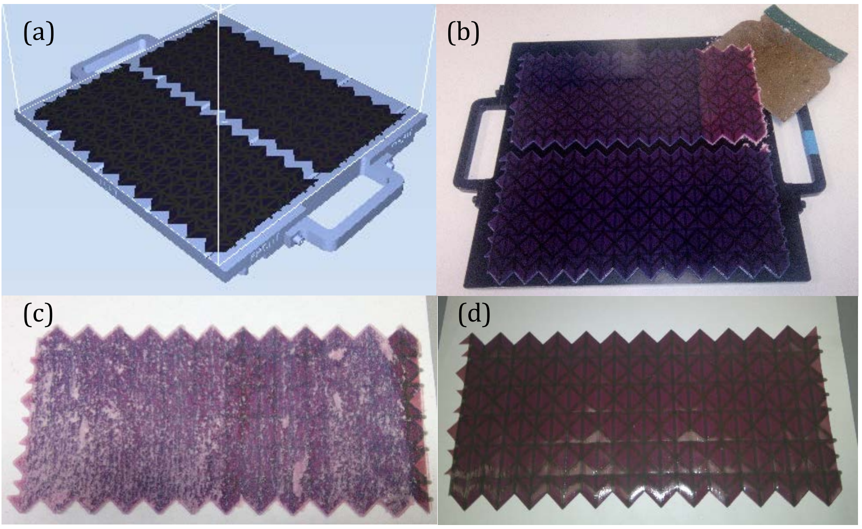

Fig. 49 Base sheet 3D Printing process (a) Sheet placing and material assignation (b) removing the 3D printed sheet from the printer's tray (c) the support material has to be scraped from the 3D printed sheet (d) Final base sheet after 3D printing and cleaning

2. Once the base sheet has been printed and cleaned, the short margins are glued together to form a cylinder using J-B Weld Plastic Bonder. This glue must be left at least one hour to dry properly. The result is an airtight bond which maintains the properties of the hinge.

3. Finally, the cylindrical surface is closed and sealed by gluing together the end rhomboidal rigid panels using the same plastic bonder. Then, the two hose barb adapters are introduced in into the small entries placed at both ends of the actuator.

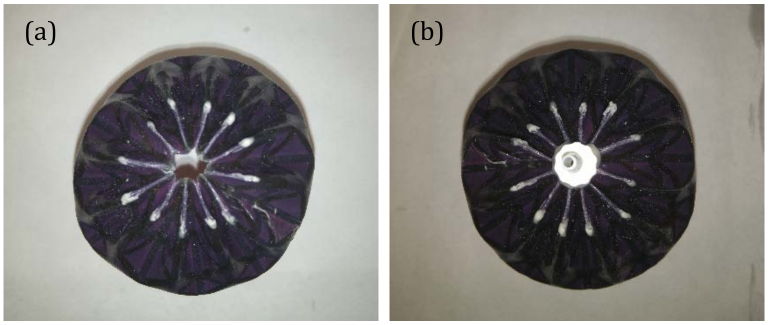

Fig. 50 3D Printed surface sealing process. (a) the rhomboidal rigid panels are glued together leaving a small entrance at each end. (b) A hose barb adapter is introduced and glued at both ends.

The airtight properties of this spheroidal enclosed surface were tested by submerging it under water. No air bubbles were detected.

After this test, we were ready to apply the thermomechanical activation on the active hinges. To do so, we intended to follow the same procedure applied to the hinge samples by heating the actuator in a water bath at 80ºC, then stretching it using compressed air and cooling it in a 20ºC water bath.

However, when we plunged the actuator in hot water, the hinges became softer and the air inside the actuator excreted enough pressure to tear the surface apart (Fig. 51).

Fig. 51 Actuator broken during the thermomechanical activation process.

5.7.Redesign

This first attempt could be considered a failure, as we couldn't successfully fold the surface into the desired pattern. However, this results provided lots of information and allowed us to understand in more depth both the materials we are using and the thermomechanical activation process.

We realized that those hinges were too weak to withstand the pressure and forces we want to subject them. Furthermore, the self-bending properties of the hinges were lower than expected due to the interaction between panels.

Therefore, we decided to redesign the hinge geometry and upgrade the 3D printing and thermomechanical activation processes.

5.7.1. Hinge optimization:

Originally, the main function of the SMP fiber embedded into the elastomeric matrix was to produce the self-folding effect once the hinge was thermomechanically activated. However, we realized that these fibers developed also a structural function as the rubbery material for the elastomeric matrix is too weak to withstand the forces we are applying for himself.

In fact, the hinges usually break when a fiber fails. The rubbery material can break without compromising the hinge. However, once a fiber has been broken, the generated crack can travel across the surface, tearing it easily.

Therefore, in order to create a more reliable hinge structure, we decided to use a continuous SMP lamina instead of fibers (Fig. 52).

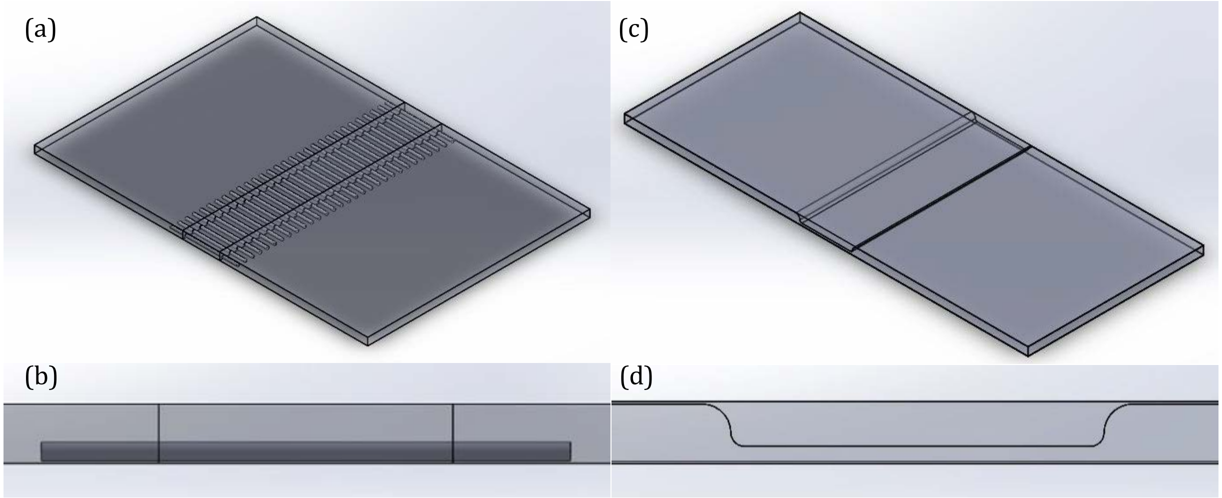

Fig. 52 Comparison between hinges with embedded fibers and continuous lamina. (a) Fiber reinforced hinge design (b) Side detail of the fiber reinforced hinge (c) Continuous lamina hinge design (d) Side detail of the continuous lamina hinge.

In the original design, three materials were used: a rigid material for the fibers (RGD-MK-K10-DM) a rubbery material for the elastomeric matrix (TangoBlackPlus) and a rigid material for the rigid panels (RGD-MK-K60-DM). As it can be seen in Fig. 52 (b), there is not a smooth transition between the rigid panels and the elastomeric matrix.

In the new design, we are suggesting a hinge geometry that only relies on two materials: an inner core of a rigid material like VeroMagenta or RGD-MK-K10-DM and an external layer of TangoBlackPlus. These two layers are continuous across all the surface and the rigid panels and hinges can be created by modifying the proportion of rigid and rubbery materials while keeping the thickness of the sheet constant.

The main idea behind this new design is to make the hinges less likely to tear apart while improving their self-folding properties. A continuous SMP layer should strengthen the hinges and make them more reliable. Furthermore, in section 5.4.2 we proved that a higher fiber density lead to an increase in the angle achieved by the hinge. Therefore, a continuous layer of SMP should improve the bending properties.

On the other hand, the thin layer of rubbery material on the rigid panels should give a soft touch while improving the airtightness of the actuator.

Some tests are required to figure out the optimal proportion of rubbery and rigid material for the hinges. Unfortunately, the department that owns the 3D printer we are using ran out of VeroMagenta (and other materials from the Vero family) and they won't be buying new material on time for this project.

5.7.2. 3D Printing optimization:

From the beginning, we realized that the 3D printed samples were sticky just after printing them. We ran all tests in section 5.4 hours or just a few days after printing the samples. However, we kept some of these samples. After some time, we realized that they have dried, losing the original stickiness and becoming harder.

We repeated the thermomechanical activation process with these remaining samples and we obtained significantly better results. Fig. 53 shows a comparison of the achieved hinge angle after 3 hours for the fiber length test (see Fig. 42) for samples just printed and samples dried out.

It can be observed how the achieved angle increased considerably, up to 27º in the case where the fibers are embedded 1mm in the rigid panels.

We also tested other samples, like the 5mm hinge samples with RGD-MK-K30-DM and RGD-MK-K40-DM fiber material. The achieved angle after 3 hours was 108º and 124º respectively. This supposes an increase of 45º and 37º in the achieved angle respect the original results (see Fig. 38).

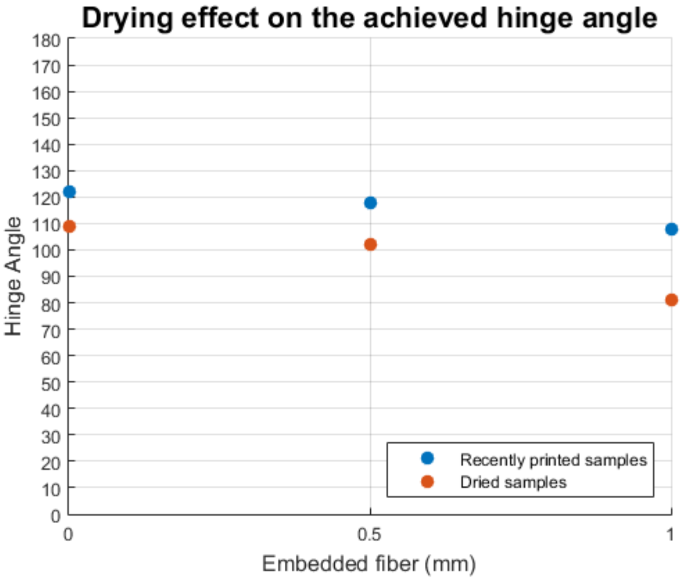

Fig. 53 Comparison of the achieved angle for recently printed samples and dried samples. This samples are the ones used for the fiber length case with RGD-MK-K60-DM as the material for the rigid panels

These results lead us to think that a post-curing process could be applied to the 3D printed models. This post-curing process could be done by exposition to UV light (as the used materials are photopolymers) or temperature.

However, it must be said that the dried samples are considerably more rigid that the original ones, being more susceptible to tear apart during the thermomechanical activation process.

Furthermore, it is also important to mention that, when preparing the setting for the 3D printing process, we always chose a setting called “Glossy finish” which is in part the reason why the samples surface was sticky. However, there is another option which is “Matte finish” that we haven’t tried because it takes more printing time and make the samples more expensive. It could be interesting to test some samples with this feature activated.

5.7.3. Thermomechanical process optimization:

As we mentioned earlier, we tested the airtightness of the spheroidal closed surface by submerging it under water without any problem. However, when we plunged the actuator in the hot water bath, the force exerted by the enclosed air teared apart the softened hinges. Therefore, we think that the best option to heat the surface should be an oven at the specified temperature. Then the cooling process could be done by the pressurized air used to stretch the hinges and also a water bath at 20ºC.

6. CONCLUSSIONS

It could be said that we failed on achieving this project main goal as we have not been able to 3D print and test the designed pneumatic artificial muscle. It must be said, though, that the lack of 3D printing material availability is what limited us.

However, we can conclude that that we achieved all the other objectives.

After revising all the current technologies on PMAs and SPAs and understanding the limitations of the 3D printer we understood that we needed to design an actuator which ability to contract rely on a rearranging membrane.

We designed an origami-based actuator that uses the waterbomb pattern to operate. This geometry has the ability to contract upon inflation while keeping the surface area constant. The fact that the actuator doesn't rely on a stretching membrane should reduce the pressure threshold and hysteresis problems associated with common PMS as well as make it more reliable.

We tested different variations of the waterbomb pattern using paper prototypes coated with silicone. These experiments showed us that he 4x8 cell configuration can't be used as an artificial muscle. However, both 6x12 and 8x16 configuration behaved like PAMs. We tested these actuators under 2, 4 and 7N loads, achieving a maximum contraction ratio of 12.446 for the 92.84mm long 8x16 cardboard-based actuator. The maximum operating pressure was 4.682Pa for the cardboard-based configuration under 7N.

We also concluded that these results could be improved if the end caps were specially designed to seal properly the actuator while transmitting efficiently the forces from the membrane to the load. We estimate that the maximum contraction ratio should be between 15% and 20% of the original length.

These results also showed some hysteresis in the inflation and deflation processes. However, these results are obtained from transitory states. We believe that this hysteresis can be reduced if the data is recorded for stationary states.

When we tried to 3D print this actuator, we quickly realized about the complications of producing the final geometry directly. Therefore, we proposed to 3D print a flat structure that can self-assemble into the desired geometry using a technology termed Thermomechanically activated 4D printing.

The first attempt to self fold the actuator failed due to several deficiencies in the design, production and activation process. We proposed an optimized geometry for the hinges as well as we adapted the production and activation processes. However, we were able to test this new design due to the lack of SMP material.

7. FUTURE WORK

The next steps should be focused on testing and optimizing the new hinge design. First, some tests should be performed to identify the optimal geometry for both the hinges and the rigid panels. Furthermore, other harder rubbery materials could be tested on the elastomeric matrix to see if the hinges mechanical properties can be increased.

Once the hinge geometry is optimized, a new actuator design should be modeled, printed and tested.

It is important to mention that before creating a new SolidWorks model, the end cap problem should be solved. The hose barb adapters used in this project couldn't be held efficiently in place so they were the main cause of failure.

These new end caps should be able to act as an air inlet as well as transferring the force from the actuator to the loads without impairing the actuator's ability to contract. Furthermore, these end caps should have embedded a pressure sensor so the pressure can be recorded inside the actuator.

On the other hand, it could be also interesting to explore other fabrication processes to produce this actuator. The Daerden PPAM have some similitudes with our design so it could be possible to adapt their production process to our geometry. Both the design and fabrication process of this Daerden actuator has been improved the recent years so there is information about three different versions of this design: PPAM 1.0[28], PPAM 2.0[72] and PPAM 3.0[73]. Any of the production methods used to produce these actuators could be potentially adapted to our needs.

BIBLIOGRAPHY

1. Calisti, M. *et al.* An octopus-bioinspired solution to movement and manipulation for soft robots. *Bioinspir. Biomim.* **6,** 36002 (2011).
2. Laschi, C. *et al.* Soft Robot Arm Inspired by the Octopus. *Adv. Robot.* **26,** 709–727 (2012).
3. Shepherd, R. F. *et al.* Multigait soft robot. *Proc. Natl. Acad. Sci.* **108,** 20400–20403 (2011).
4. Tolley, M. T. *et al.* A Resilient, Untethered Soft Robot. *Soft Robot.* **1,** 213–223 (2014).
5. Ilievski, F., Mazzeo, A. D., Shepherd, R. F., Chen, X. & Whitesides, G. M. Soft robotics for chemists. *Angew. Chemie - Int. Ed.* **50,** 1890–1895 (2011).
6. Marchese, A. D., Onal, C. D. & Rus, D. Autonomous Soft Robotic Fish Capable of Escape Maneuvers Using Fluidic Elastomer Actuators. *Soft Robot.* **1,** 75–87 (2014).
7. Polygerinos, P. *et al.* Towards a soft pneumatic glove for hand rehabilitation. *IEEE Int. Conf. Intell. Robot. Syst.* 1512–1517 (2013). doi:10.1109/IROS.2013.6696549
8. Polygerinos, P., Wang, Z., Galloway, K. C., Wood, R. J. & Walsh, C. J. Soft robotic glove for combined assistance and at-home rehabilitation. *Rob. Auton. Syst.* **73,** 135–143 (2015).
9. Yap, H. K., Lim, J. H., Nasrallah, F., Goh, J. C. H. & Yeow, R. C. H. A soft exoskeleton for hand assistive and rehabilitation application using pneumatic actuators with variable stiffness. *Proc. - IEEE Int. Conf. Robot. Autom.* **2015–June,** 4967–4972 (2015).
10. Yap, H. K., Ang, B. W. K., Lim, J. H., Goh, J. C. H. & Yeow, C. H. A fabric-regulated soft robotic glove with user intent detection using EMG and RFID for hand assistive application. *Proc. - IEEE Int. Conf. Robot. Autom.* **2016–June,** 3537–3542 (2016).
11. Doumit, M., Fahim, A. & Munro, M. Analytical modeling and experimental validation of the braided pneumatic muscle. *IEEE Trans. Robot.* **25,** 1282–1291 (2009).
12. Tondu, B. Modelling of the McKibben artificial muscle: A review. *J. Intell. Mater. Syst. Struct.* **23,** 225–253 (2012).
13. Daerden, F. & Lefeber, D. Pneumatic artificial muscles: actuators for robotics and automation. *Eur. J. Mech. Environ. Eng.* **47,** 11–21 (2002).
14. Payter, M. H. High pressure fluid-driven tension actuators and method for constructing them, US Patent No. 4751869. (1988).
15. Klute, G. K., Czerniecki, J. M. & Hannaford, B. McKibben artificial muscles: pneumatic actuators with biomechanical\nintelligence. *1999 IEEE/ASME Int. Conf. Adv. Intell. Mechatronics (Cat. No.99TH8399)* 1–6 (1999). doi:10.1109/AIM.1999.803170
16. Kang, B. S., Kothera, C. S., Woods, B. K. S. & Wereley, N. M. Dynamic modeling of mckibben pneumatic artificial muscles for antagonistic actuation. *Proc. - IEEE Int. Conf. Robot. Autom.* 182–187 (2009). doi:10.1109/ROBOT.2009.5152280
17. Meller, M. a., Bryant, M. & Garcia, E. Reconsidering the McKibben muscle: Energetics, operating fluid, and bladder material. *J. Intell. Mater. Syst. Struct.* **25,** 2276–2293 (2014).
18. Shadow 30mm Air Muscle Datasheet. (2011).
19. Zhao, J., Zhong, J. & Fan, J. Position control of a pneumatic muscle actuator using RBF-Neural Network tuned PID controller. **2015,** (2015).
20. Wu, J., Huang, J., Wang, Y., Xing, K. & Xu, Q. Fuzzy PID control of a wearable rehabilitation robotic hand driven by pneumatic muscles. *20th Anniv. MHS 2009 Micro-Nano Glob. COE - 2009 Int. Symp. Micro-NanoMechatronics Hum. Sci.* 408–413 (2009). doi:10.1109/MHS.2009.5352012
21. Medrano-Cerda, G. A. ., Bowler, C. J. . & Caldwell, D. G. . Adaptive Position Control of Antagonistic Pneumatic Muscle Actuators. *Intell. Robot. Syst.* **1,** 378–383 (1995).
22. Sárosi, J., Gyeviki, J., Véha, A. & Toman, P. Accurate position control of PAM actuator in LabVIEW environment. *SISY 2009 - 7th Int. Symp. Intell. Syst. Informatics* 301–305 (2009). doi:10.1109/SISY.2009.5291145
23. Ching-Ping Chou & Hannaford, B. Measurement and modeling of McKibben pneumatic artificial muscles. *IEEE Trans. Robot. Autom.* **12,** 90–102 (1996).
24. Zhong, J., Fan, J., Zhu, Y., Zhao, J. & Zhai, W. Static modeling for commercial braided pneumatic muscle

actuators. *Adv. Mech. Eng.* **2014,** (2014).

25. Yarlott, J. M. Fluid Actuator, US Patent No. 3645173. (1972).
26. Kukolj, M. & Immega, G. Axially Contractable Actuator, US Patent No. 4939982. (1990).
27. Kukolk, M. Axially Contrcatable Actuator, US Patent No. 4733603. (1988).
28. Daerden, F. Conception and Realization of Pleated Pneumatic Artificial Muscles and their Use as Compliant Actuation Elements. (1999).
29. Baldwin, H. A. Realizable models of muscle function. *Proc. First Rock Biomech. Symp.* 139–148 (1969).
30. Paynter, M. H. Hyperboloid of revolution fluid-driven tension actuators and method of marking, US Patent No. 4721030. (1988).
31. Sun, Y., Song, Y. S. & Paik, J. Characterization of silicone rubber based soft pneumatic actuators. *IEEE Int. Conf. Intell. Robot. Syst.* 4446–4453 (2013). doi:10.1109/IROS.2013.6696995
32. Yao, L. *et al.* PneUI: Pneumatically Actuated Soft Composite Material s for Shape Changing Interfaces. *Proc. 26th Annu. ACM Symp. User interface Softw. Technol. - UIST '13* 13–22 (2013). doi:10.1145/2501988.2502037
33. Mosadegh, B. *et al.* Pneumatic networks for soft robotics that actuate rapidly. *Adv. Funct. Mater.* **24,** 2163–2170 (2014).
34. Polygerinos, P. *et al.* Modeling of Soft Fiber-Reinforced Bending Actuators. *IEEE Trans. Robot.* **31,** 778–789 (2015).
35. Deimel, R. & Brock, O. A compliant hand based on a novel pneumatic actuator. *Proc. - IEEE Int. Conf. Robot. Autom.* 2047–2053 (2013). doi:10.1109/ICRA.2013.6630851
36. Deimel, R. & Brock, O. A novel type of compliant and underactuated robotic hand for dexterous grasping. *Int. J. Rob. Res.* **35,** 161–185 (2016).
37. Park, Y.-L., Majidi, C., Kramer, R., Bérard, P. & Wood, R. J. [37]Hyperelastic pressure sensing with a liquid-embedded elastomer. *J. Micromechanics Microengineering* **20,** 125029 (2010).
38. Stokes, A. a, Shepherd, R. F., Morin, S. a, Ilievski, F. & Whitesides, G. M. A Hybrid Combining Hard and Soft Robots. *Soft Robot.* **1,** 70--74 (2014).
39. Keiko Ogura *et al.* Micro pneumatic curling actuator - Nematode actuator -. *2008 IEEE Int. Conf. Robot. Biomimetics* 462–467 (2009). doi:10.1109/ROBIO.2009.4913047
40. Wakimoto, S., Suzumori, K. & Ogura, K. Miniature Pneumatic Curling Rubber Actuator Generating Bidirectional Motion with One Air-Supply Tube. *Adv. Robot.* **25,** 1311–1330 (2011).
41. Galloway, K. C., Polygerinos, P., Walsh, C. J. & Wood, R. J. Mechanically programmable bend radius for fiber-reinforced soft actuators. *2013 16th Int. Conf. Adv. Robot. ICAR 2013* (2013). doi:10.1109/ICAR.2013.6766586
42. Konishi, S., Kawai, F. & Cusin, P. Thin flexible end-effector using pneumatic balloon actuator. *Sensors Actuators, A Phys.* **89,** 28–35 (2001).
43. Niiyama, R., Rus, D. & Kim, S. Pouch Motors: Printable/inflatable soft actuators for robotics. *Proc. - IEEE Int. Conf. Robot. Autom.* 6332–6337 (2014). doi:10.1109/ICRA.2014.6907793
44. Peraza-Hernandez, E. A., Hartl, D. J., Malak Jr, R. J. & Lagoudas, D. C. Origami-inspired active structures: a synthesis and review. *Smart Mater. Struct.* **23,** 94001 (2014).
45. Naboni, R. & Mirante, L. Metamaterial computation and fabrication of auxetic patterns for architecture. 129–136 (2010). doi:10.5151/despro-sigradi2015-30268
46. Kuribayashi, K. *et al.* Self-deployable origami stent grafts as a biomedical application of Ni-rich TiNi shape memory alloy foil. *Mater. Sci. Eng. A* **419,** 131–137 (2006).
47. Song, Z. Studies of Origami and Kirigami and Their Applications. (2016).
48. Cagdas, D. *et al.* Towards printable robotics : Origami-inspired planar fabrication of three-dimensional mechanisms The MIT Faculty has made this article openly available . Please share Citation Printable Robotics : Origami-Inspired Planar Fabrication of Three- Accessed Cit. (2015).
49. Lee, D.-Y., Kim, J.-S., Kim, S.-R., Koh, J.-S. & Cho, K. The deformable wheel robot using magic-ball origami structure. *Proc. ASME 2013 Int. Des. Eng. Tech. Conf. Comput. Inf. Eng. Conf. IDETC/CIE 2013* 1–9 (2013). doi:10.1115/DETC2013-13016
50. Hanna, B. H. Modeling and Testing of Bistable Waterbomb Base Configurations. (2014).
51. Hanna, B. H., Lund, J. M., Lang, R. J., Magleby, S. P. & Howell, L. L. Waterbomb base: a symmetric single-vertex bistable origami mechanism. *Smart Mater. Struct.* **23,** 94009 (2014).

52. Chen, Y., Feng, H., Ma, J., Peng, R. & You, Z. Symmetric waterbomb origami. *Proc. R. Soc. A Math. Phys. Eng. Sci.* **472,** 20150846 (2016).
53. Bowen, L. *et al.* Development and Validation of a Dynamic Model of Magneto-Active Elastomer Actuation of the Origami Waterbomb Base. *J. Mech. Robot.* **7,** 11010 (2015).
54. Martinez, R. V., Fish, C. R., Chen, X. & Whitesides, G. M. Elastomeric origami: Programmable paper-elastomer composites as pneumatic actuators. *Adv. Funct. Mater.* **22,** 1376–1384 (2012).
55. Felton, S. M., Tolley, M. T., Onal, C. D., Rus, D. & Wood, R. J. Robot self-assembly by folding: A printed inchworm robot. *Proc. - IEEE Int. Conf. Robot. Autom.* 277–282 (2013). doi:10.1109/ICRA.2013.6630588
56. Felton, S., Tolley, M., Demaine, E., Rus, D. & Wood, R. A method for building self-folding machines. *Science (80-.).* **345,** 644–646 (2014).
57. Miyashita, S., Guitron, S., Ludersdorfer, M., Sung, C. R. & Rus, D. An Untethered Miniature Origami Robot that Self-folds, Walks, Swims, and Degrades. *2015 Ieee Int. Conf. Robot. Autom.* 1490–1496 (2015).
58. Liu, Y., Boyles, J. K., Genzer, J. & Dickey, M. D. Self-folding of polymer sheets using local light absorption. *Soft Matter* **8,** 1764–1769 (2012).
59. Ryu, J. *et al.* Photo-origami-Bending and folding polymers with light. *Appl. Phys. Lett.* **100,** 16–21 (2012).
60. Campbell, T. a., Tibbits, S. & Garrett, B. The Next Wave : 4D Printing Programming the Material World. *Atl. Counc.* (2014).
61. Khoo, Z. X. *et al.* 3D printing of smart materials: A review on recent progresses in 4D printing. *Virtual Phys. Prototyp.* **10,** 103–122 (2015).
62. Leist, S. K. & Zhou, J. Current status of 4D printing technology and the potential of light-reactive smart materials as 4D printable materials. *Virtual Phys. Prototyp.* **2759,** 1–14 (2016).
63. Tibbits, S. TED Talks - The emergence of '4D printing'. (2013).
64. Campbell, T., Tibbits, S. & Garrett, B. The Programmable World. *Sci. Am.* **311,** 60–65 (2014).
65. Raviv, D. *et al.* Active printed materials for complex self-evolving deformations. *Sci. Rep.* **4,** 7422 (2014).
66. Tibbits, S. 4D Printing: Multi-material shape change. *Archit. Des.* **84,** 116–121 (2014).
67. Ge, Q., Dunn, C. K., Qi, H. J. & Dunn, M. L. Active origami by 4D printing. *Smart Mater. Struct.* **23,** 1–15 (2014).
68. Ge, Q., Qi, H. J. & Dunn, M. L. Active materials by four-dimension printing. *Appl. Phys. Lett.* **103,** 1–6 (2013).
69. Yu, K., Ritchie, A., Mao, Y., Dunn, M. L. & Qi, H. J. Controlled Sequential Shape Changing Components by 3D Printing of Shape Memory Polymer Multimaterials. *Procedia IUTAM* **12,** 193–203 (2015).
70. Stratasys. Stratasys PolyJet Materials Data Sheet. (2014).
71. Stratasys. Objet Additional Materials Data Sheet. (2013).
72. Verrelst, B. *et al.* Second generation pleated pneumatic artificial muscle and its robotic applications. *Adv. Robot.* **20,** 783–805 (2006).
73. Villegas, D., Van Damme, M., Vanderborght, B., Beyl, P. & Lefeber, D. Third–Generation Pleated Pneumatic Artificial Muscles for Robotic Applications: Development and Comparison with McKibben Muscle. *Adv. Robot.* **26,** 1205–1227 (2012).

APPENDIX A:

2N Test results

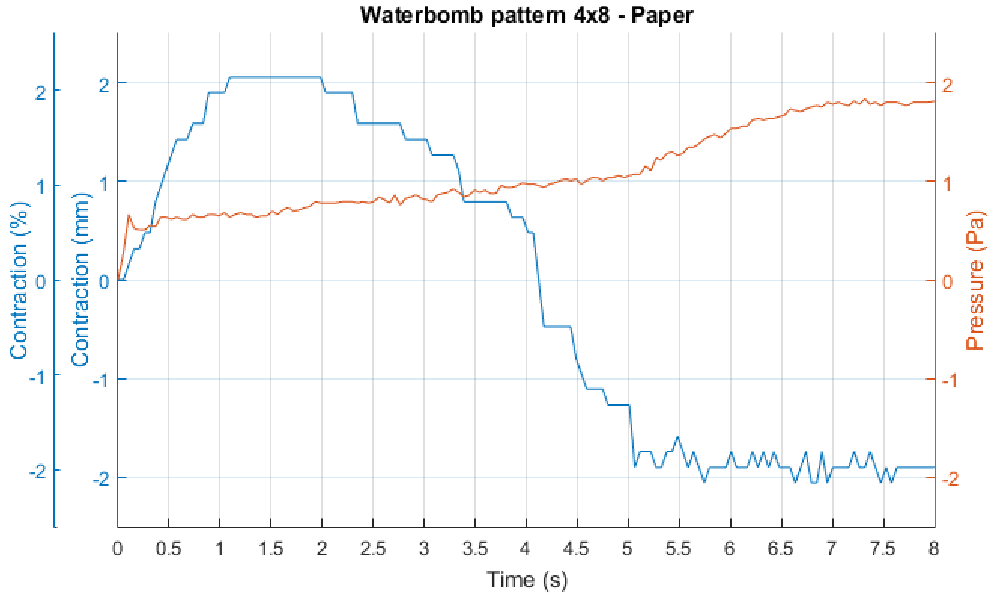

Fig. 54 Test results for the 4x8 paper-based Waterbomb actuator under a 2N load and a 75cm^3/s airflow.

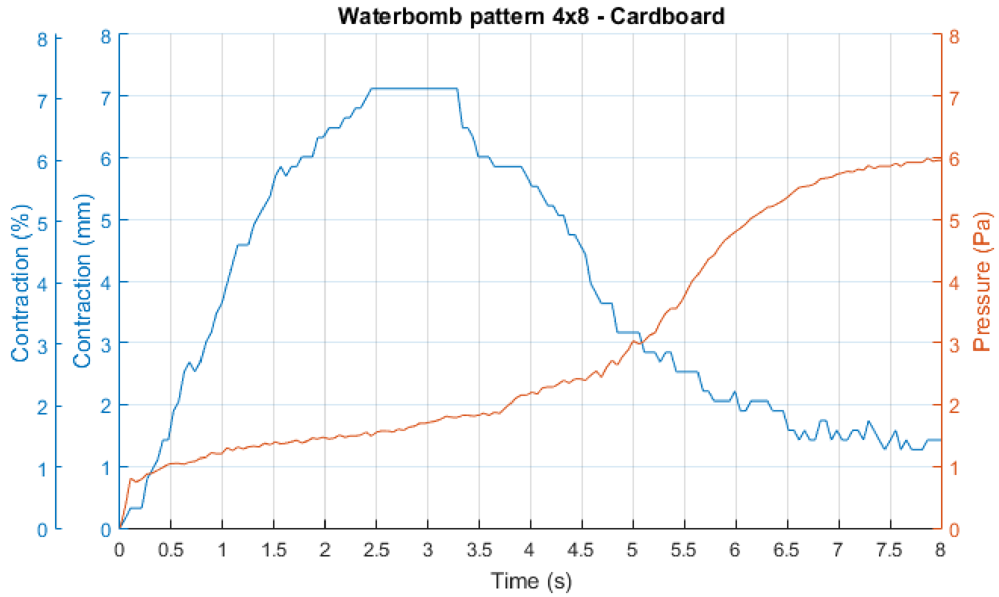

Fig. 55 Test results for the 4x8 cardboard-based Waterbomb actuator under a 2N load and a 75cm^3/s airflow.

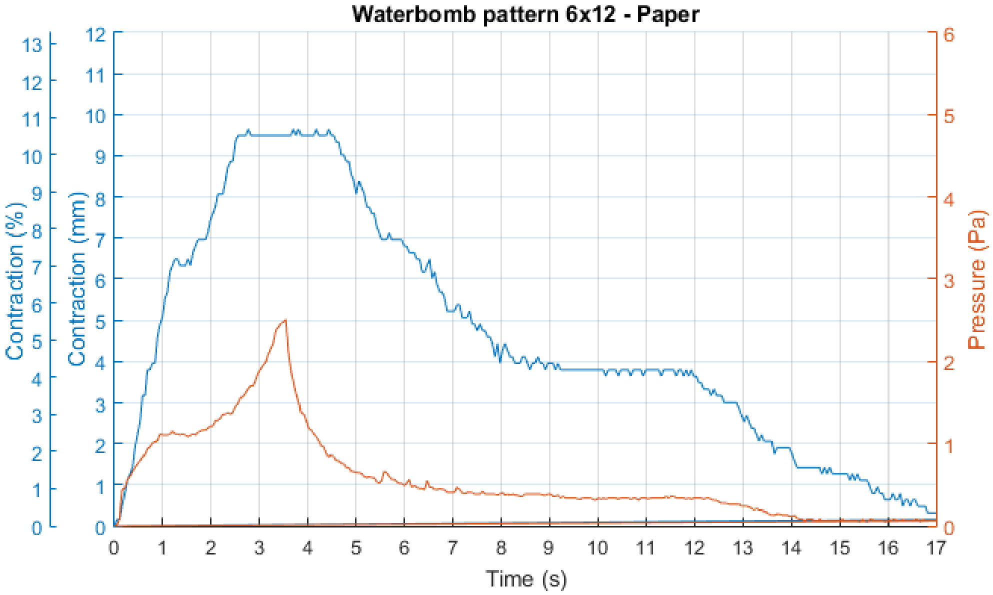

Fig. 56 Test results for the 6x12 paper-based Waterbomb actuator under a 2N load and a 75cm^3/s airflow.

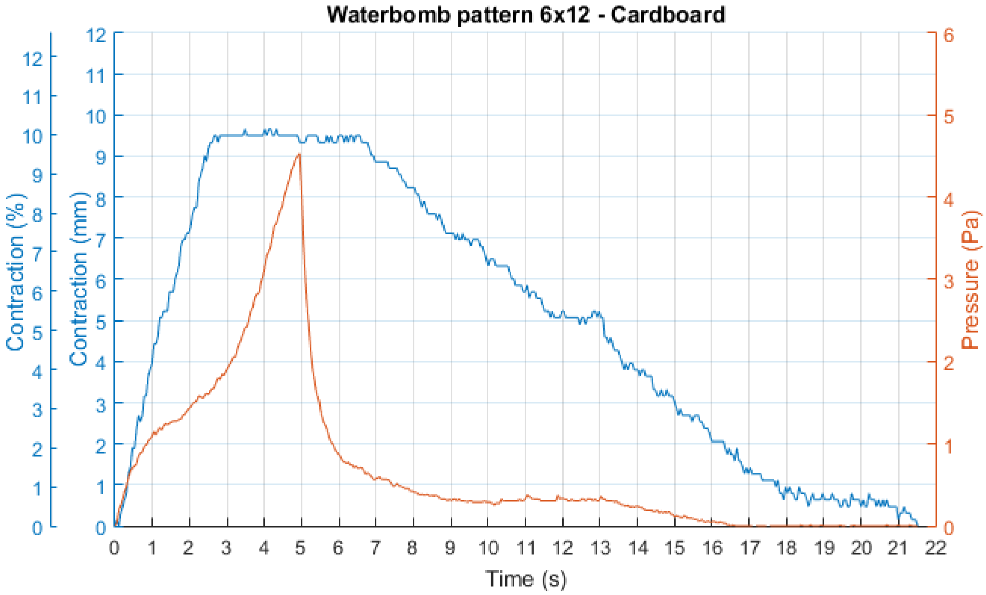

Fig. 57 Test results for the 6x12 cardboard-based Waterbomb actuator under a 2N load and a 75cm^3/s airflow.

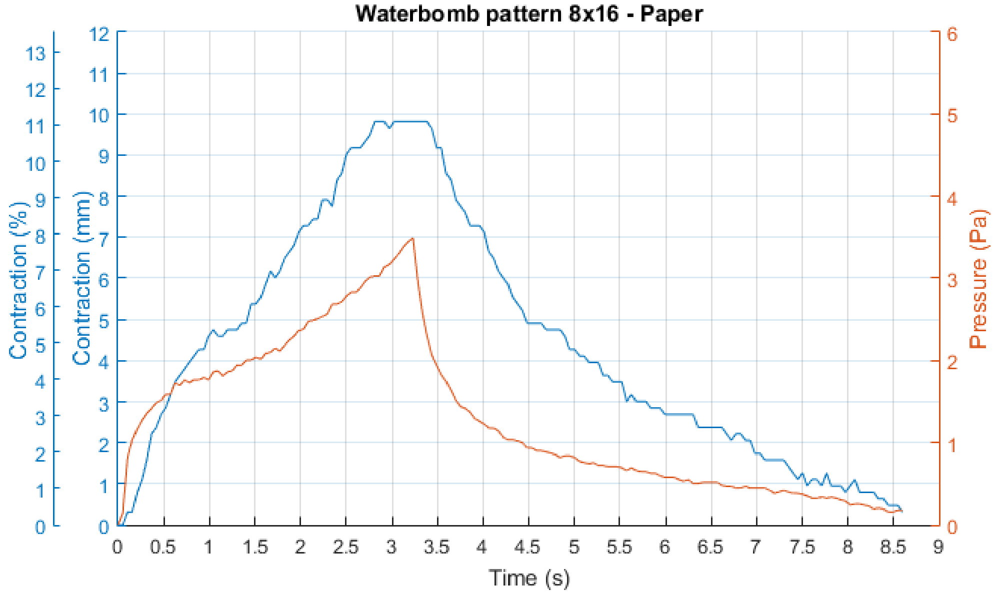

Fig. 59 Test results for the 8x16 paper-based Waterbomb actuator under a 2N load and a 75cm^3/s airflow.

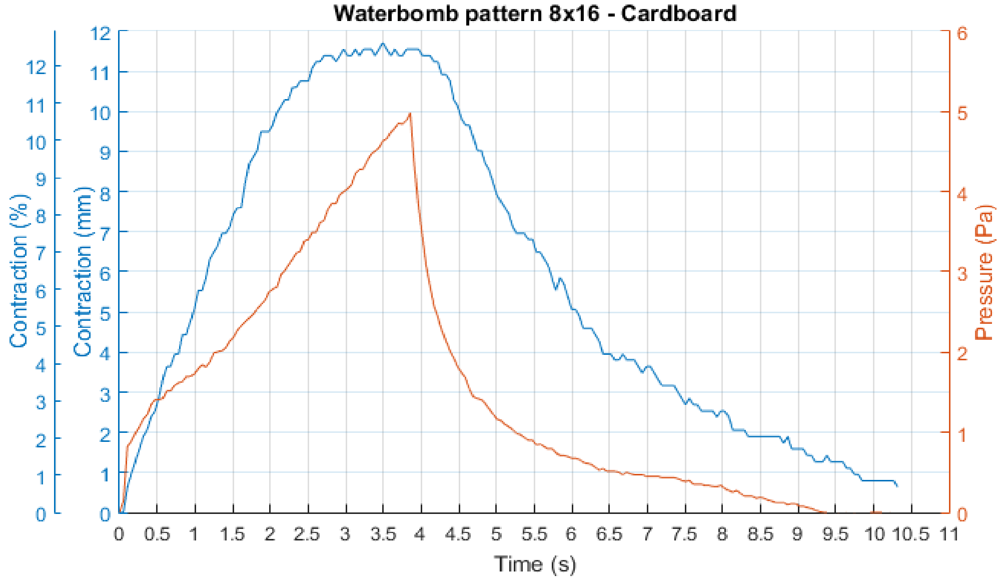

Fig. 58 Test results for the 8x16 cardboard-based Waterbomb actuator under a 2N load and a 75cm^3/s airflow.

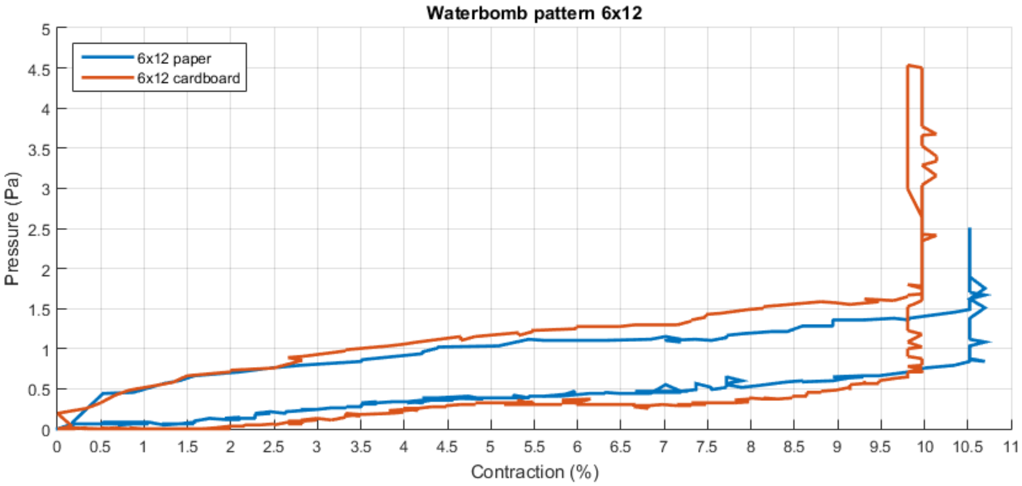

Fig. 60 Contraction vs Pressure plot for the 6x12 Waterbomb actuators under 2N and an airflow of 75cm³/s

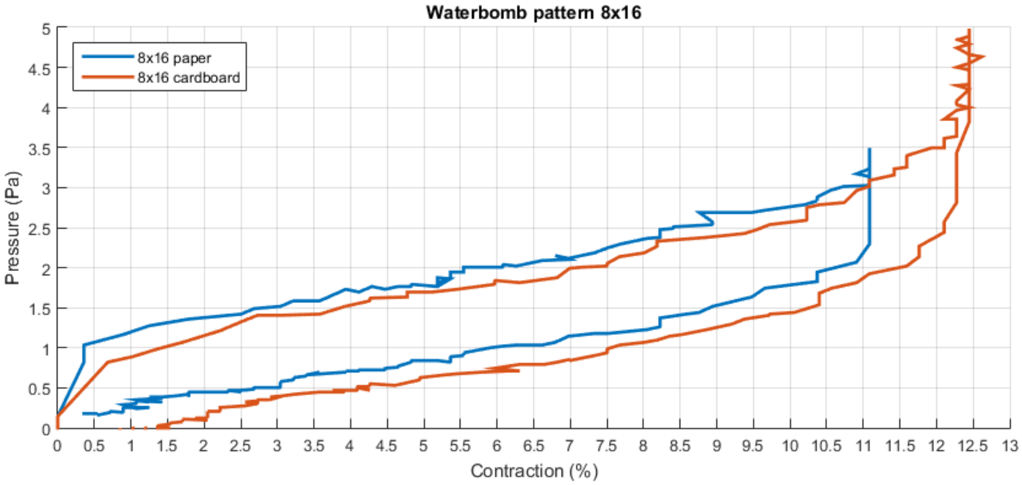

Fig. 61 Contraction vs Pressure plot for the 8x16 Waterbomb actuators under 2N and an airflow of 75cm³/s

APPENDIX B:

4N Test results

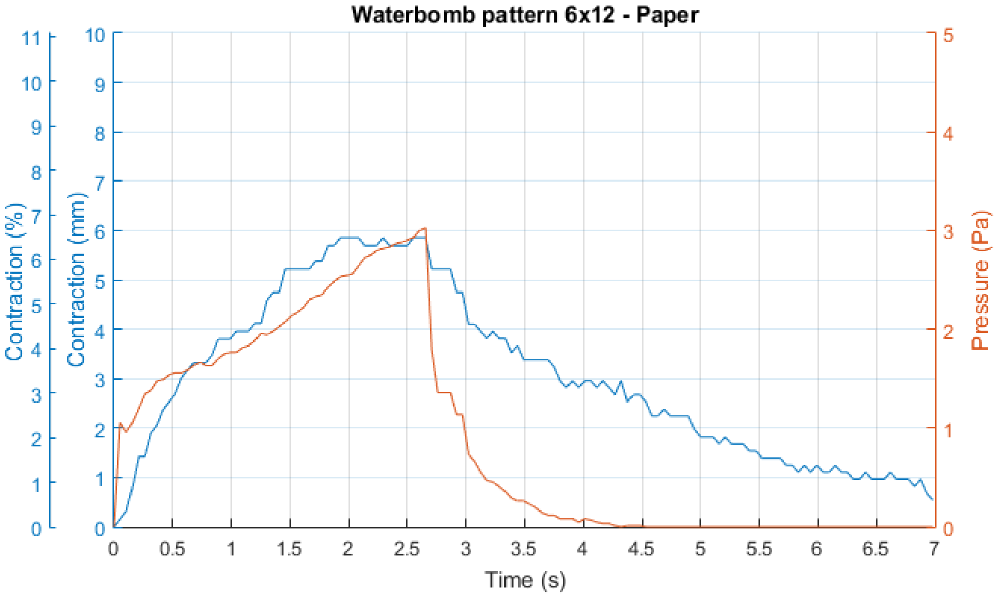

Fig. 63 Test results for the 6x12 paper-based Waterbomb actuator under a 4N load and a 90cm^3/s airflow.

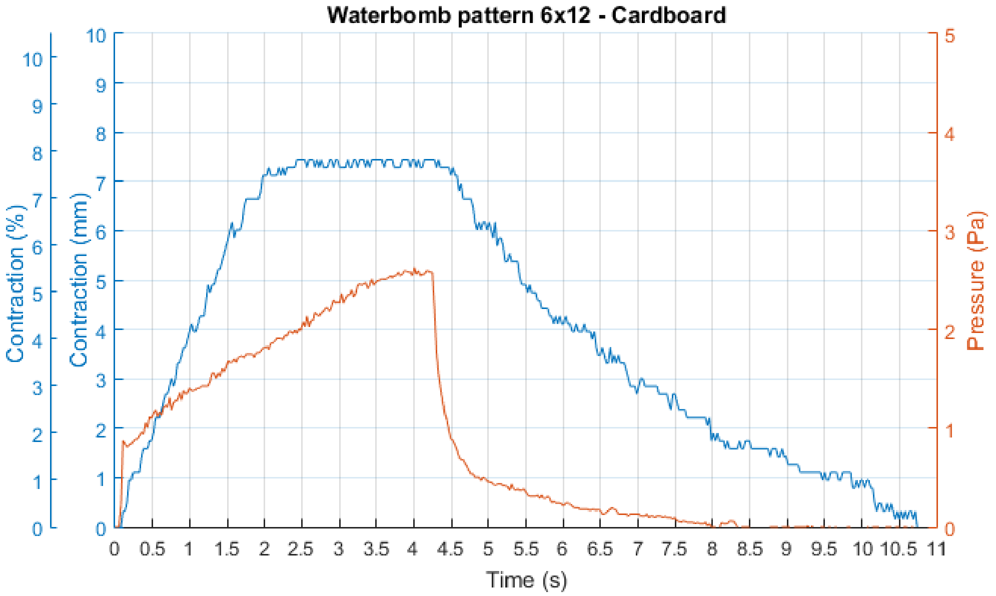

Fig. 62 Test results for the 6x12 cardboard-based Waterbomb actuator under a 4N load and a 90cm^3/s airflow.

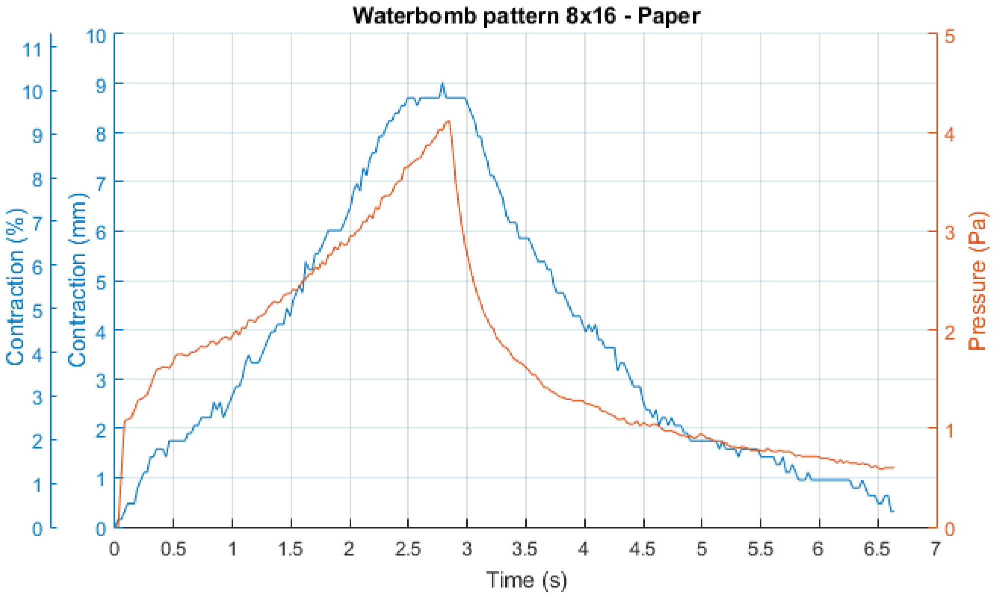

Fig. 64 Test results for the 8x16 paper-based Waterbomb actuator under a 4N load and a 90cm^3/s airflow.

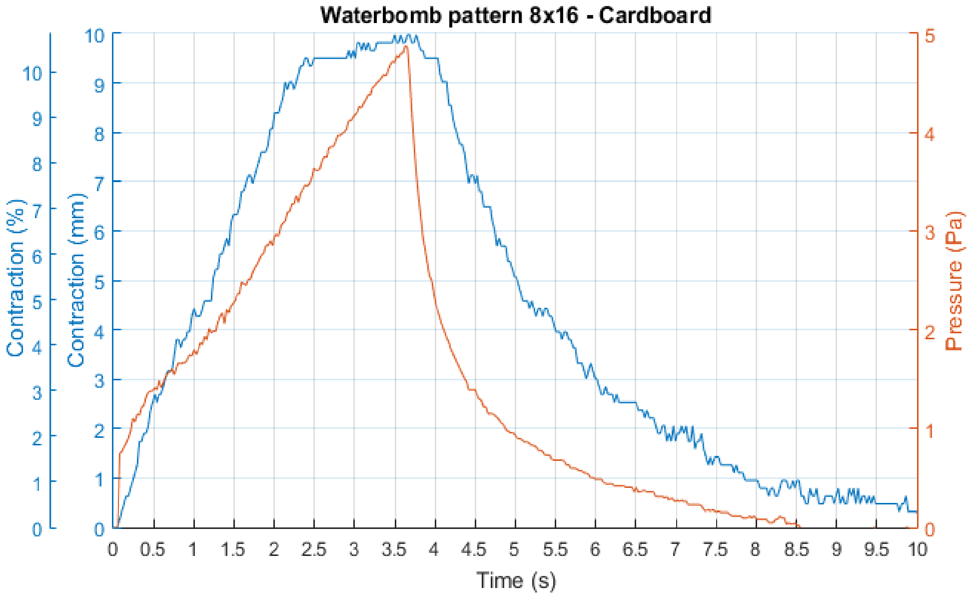

Fig. 65 Test results for the 8x16 cardboard-based Waterbomb actuator under a 4N load and a 90cm^3/s airflow.

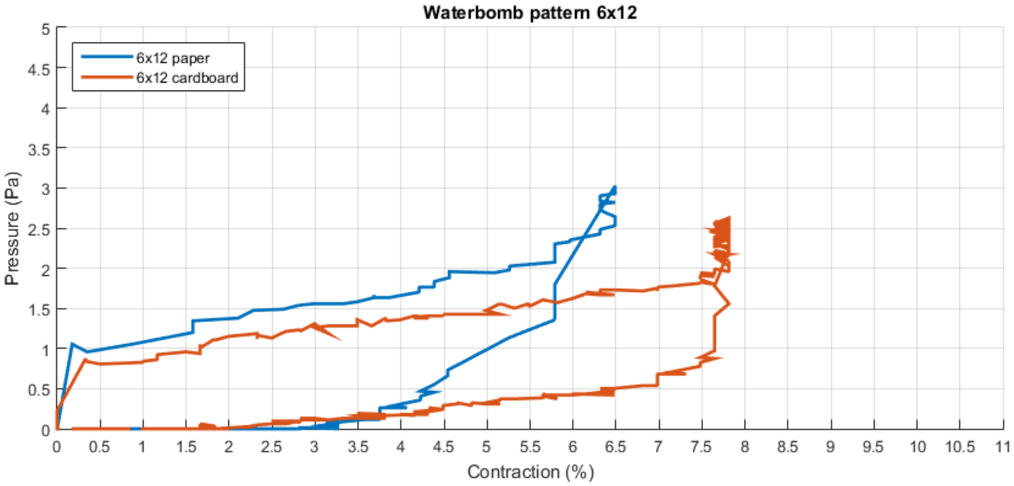

Fig. 66 Contraction vs Pressure plot for the 6x12 Waterbomb actuators under 4N and an airflow of 90cm^3/s

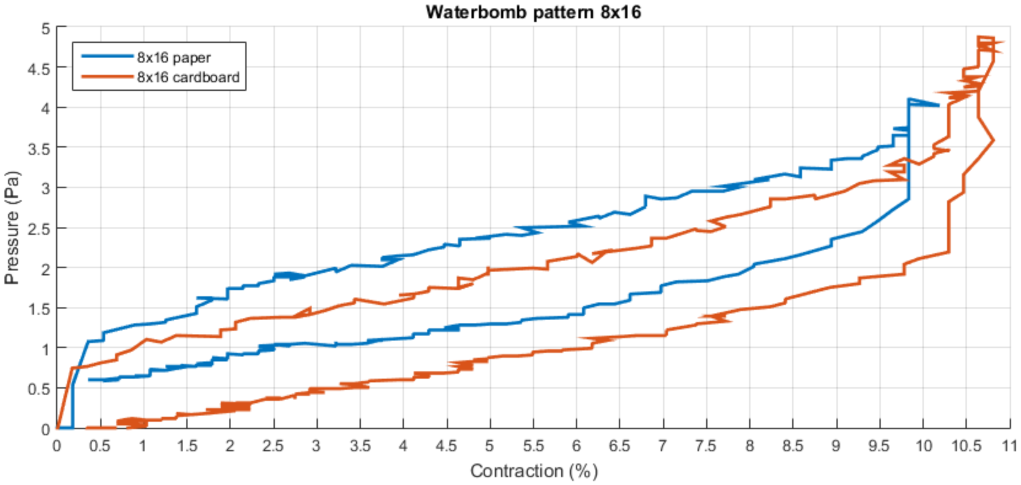

Fig. 67 Contraction vs Pressure plot for the 8x16 Waterbomb actuators under 4N and an airflow of 90cm^3/s

APPENDIX C:

7N Test results

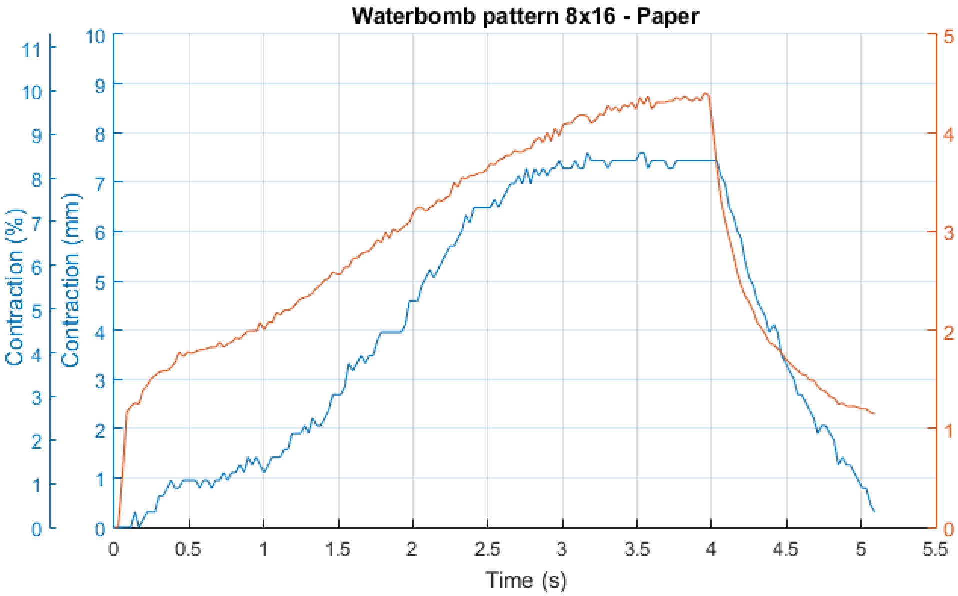

Fig. 69 Test results for the 8x16 paper-based Waterbomb actuator under a 7N load and a 90cm^3/s airflow.

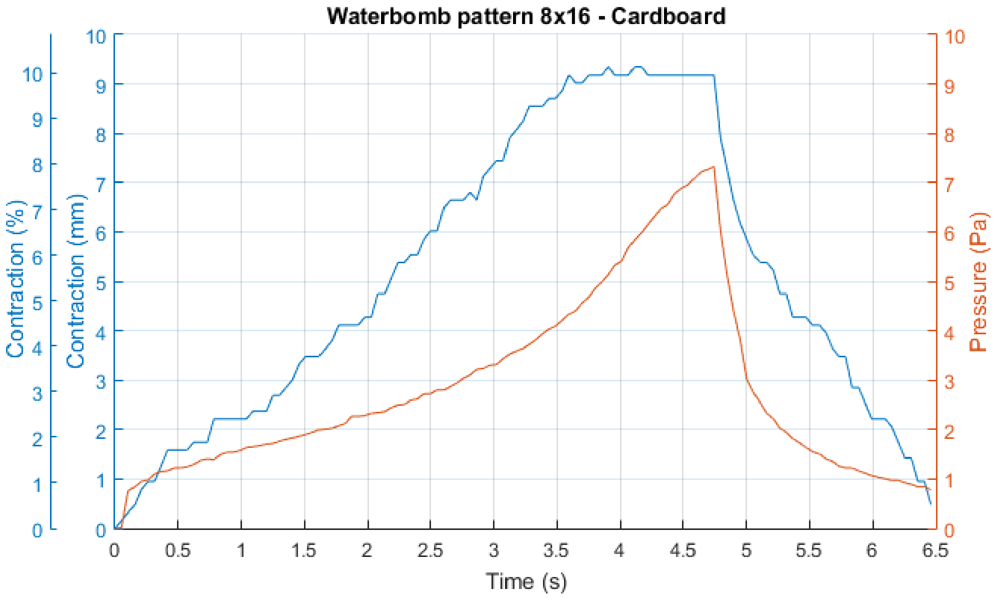

Fig. 68 Test results for the 8x16 cardboard-based Waterbomb actuator under a 7N load and a 90cm^3/s airflow.

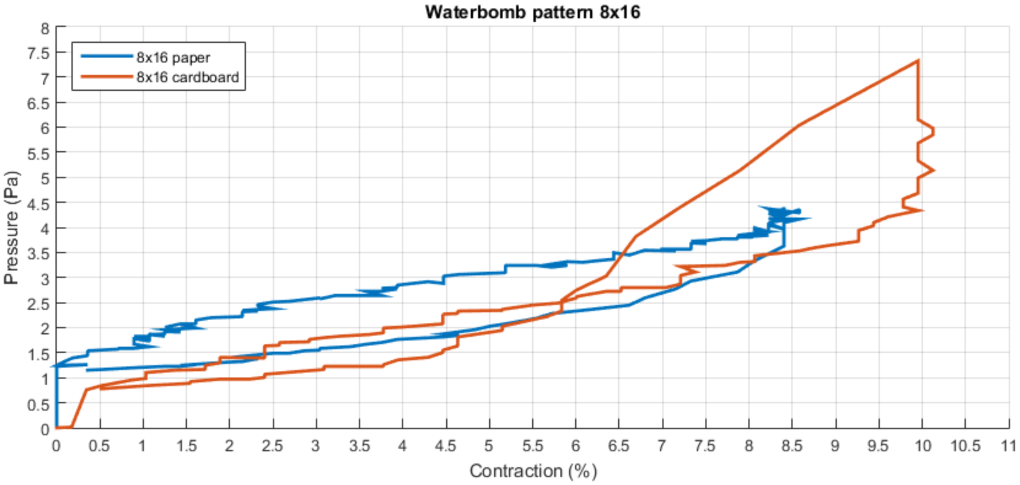

Fig. 70 Contraction vs Pressure plot for the 8x16 Waterbomb actuators under 7N and an airflow of 90cm^3/s